Summer 2022

Modeling the reactor time-dependent delayed particle tail with Monte Carlo N-Particle (MCNP) version 6.2

Eli James Boland

Department:

MODELING THE REACTOR TIME-DEPENDENT DELAYED PARTICLE TAIL WITH MONTE CARLO N-PARTICLE (MCNP) VERSION 6.2

by

ELIJAH JAMES BOLAND

A THESIS

Presented to the Graduate Faculty of the

MISSOURI UNIVERSITY OF SCIENCE AND TECHNOLOGY

In Partial Fulfillment of the Requirements for the Degree

MASTER OF SCIENCE IN NUCLEAR ENGINEERING

2022

Approved by:

Ayodeji Alajo, Advisor
Syed Alam
Edward Lum

ABSTRACT

Energy is deposited into experiment packages due to post-shutdown decay heat created from delayed particles. Modeling these delayed particles in a reactor assists researchers in quantifying the expected energy deposition sources to an experiment package before irradiation. This paper focuses on modeling the delayed particles in a reactor in MCNP6.2 by capturing a reactor as a source, converting this source capture to a source definition, applying appropriate physics such as activation and photonuclear interactions, and finally using proper tallies to create the expected delayed particle tail of a reactor.

To capture the source distribution, the FMESH capability within MCNP was used with the keyword TYPE set to SOURCE. To capture the energy distribution, an F4 tally with an E card would be applied to the reactor of interest to find the energy-dependent flux. The output MESHTAL of the FMESH and F4 tally results were then normalized and converted to a source definition. The ACT card within MCNP was utilized to create delayed particles and photonuclear interactions were turned on using the PHYS:P card. The F4 tally was utilized in tandem with T4 cards to model the time-dependent flux behavior within the reactor system which represents the delayed particle tail of the reactor.

This methodology was validated using compensating ion chamber detector data from the Missouri S&T Reactor (MSTR). The normalized trend of the MCNP F4 output agrees generally well with the normalized MSTR detector data and conservatively overestimates the normalized MSTR detector data, especially at later time bins.

ACKNOWLEDGMENTS

This project would not have been possible without the support of many people. Many thanks to my advisor, Ayodeji Alajo, who ensured I was always on track and helped make some sense of the confusion. Also, thanks to my committee member and mentor, Edward Lum, who offered a massive amount of guidance and support throughout my journey. Thanks to Michael Fensin, who assisted in explaining variance reduction methods to me. Finally, thanks to the Missouri S&T Reactor (MSTR) reactor staff Ethan Taber and Cole Kostelac who provided me with the validation data and assisted in ensuring the methodology was properly applied to the MSTR.

This material is based upon work supported under a Department of Energy, Office of Nuclear Energy, Integrated University Program Graduate Fellowship. Any opinions, findings, conclusions, or recommendations expressed in this publication are those of the author and do not necessarily reflect the views of the Department of Energy Office of Nuclear Energy.

TABLE OF CONTENTS

Page

LIST OF ILLUSTRATIONS

LIST OF TABLES

NOMENCLATURE

Nomenclature	Meaning
MCNP	Monte Carlo N-Particle
ENDF	Evaluated Nuclear Data File
DN	Delayed Neutron
GEF	A General Description of Fission Observables
CINDER	Material Burnup Calculator
ACE	A Compact ENDF
SNL	Sandia National Laboratory
ACRR	Annular Core Research Reactor
FREC-II	Fueled Ring External Cavity
KCODE	Criticality Mode
D-T	Deuterium-Tritium
ACT	Activation Card
TRIGA	Training, Research, Isotopes, General Atomics
WINCO	Westinghouse Idaho Nuclear Company
β_{eff}	Effective Delayed Neutron Fraction
dnb	Delayed Neutron Bias
PHYS:N	Neutron Physics Card
SSW/SSR	Surface Source Write/Surface Source Read
MPI	Message Passing Interface
HPC	High-Performance Computing

MESHTAL	FMESH Tally Output File
T4	Time Cell Flux Card
MODE	Particle Transport Card
PHYS:P	Photon Physics Card
MXm	Nuclide Substitution Card
NPS	Number of Particle Histories
MPHYS	Model Physics Card
FOM	Figure of Merit
WWG	Weight Window Generator Card
TSPLT	Time Split Card
CUT	Physics Cutoff Card
DXTRAN	Deterministic Transport Sphere Card
WWOUT	Weight Window Generator Output File
MESH	Superimposed Importance Mesh
WWP	Weight Window Parameter Card
MSTR	Missouri S&T Reactor
CIC	Compensating Ion Chamber
MTR	Materials Test Reactor
CAE	Core Access Element
CPU	Central Processing Unit
UIC	Uncompensated Ion Chamber
F6	Cell Energy Deposition Tally

1. INTRODUCTION

1.1. THE PROBLEM AND GOAL

Experiments irradiated in a reactor receive energy post-shutdown due to decay heat created from delayed particles. Figures 1.1 and 1.2 illustrate this impact for both a pulse and steady-state reactor, respectively. This decay heat is created by the delayed gammas and neutrons within the system. Most of these delayed particles are created either by the decay of fission fragments or by the activation of materials within the reactor. This energy deposition into the package is difficult to estimate yet must be accounted for to ensure that the desired amount of energy is deposited to the experiment package. Most often the impact of this delayed particle tail is unavoidable as most experimental facilities at a reactor do not allow for the ability to remove an experiment at the exact time of prompt shutdown.

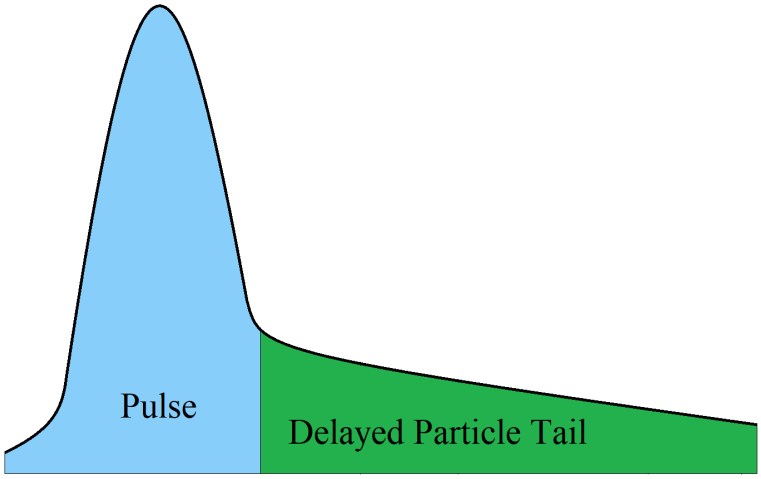

Figure 1.1 Delayed Particle Tail in a Pulse Reactor [1]

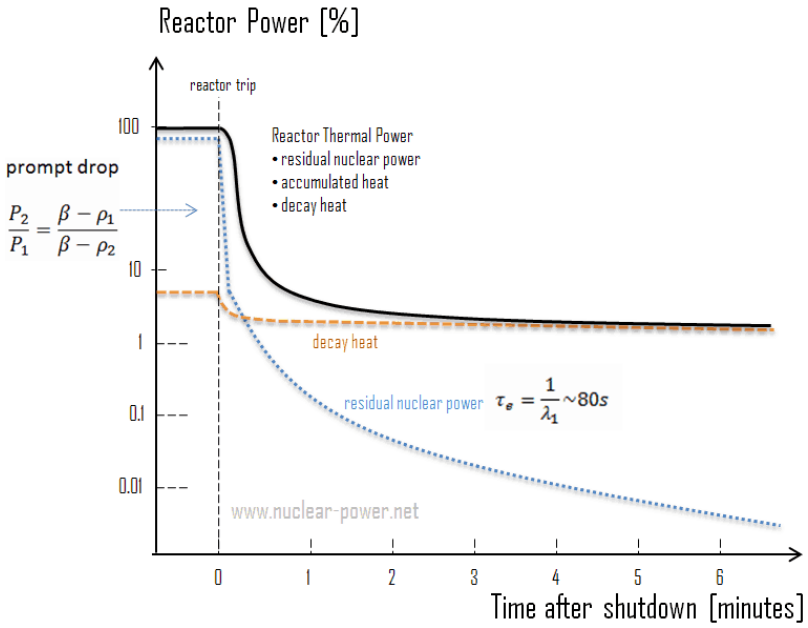

Figure 1.2 Delayed Particle Tail in a Steady-State Reactor [2]

For pulse reactors especially, this energy deposited into an experiment creates uncertainty in the temperature response from the pulse versus the pulse's delayed tail [1]. Latent energy deposition that is unaccounted for means when experiment packages are analyzed, it is unknown if any defects are from the dose rate of the pulse or the integral of the delayed particles [1]. Currently, the only method to estimate the reactor decay heat applied to an experiment is to measure the temperature of a sample, but the temperature is a convolution of the pulse deposition and the delayed particles [1]. Thus, it is desired to better understand the amount of energy being deposited post-pulse [1]. This will allow experimenters to estimate the percentage of fissions from the pulse itself versus the delayed particles in experiments with fissionable material [1]. The source term in a pulse reactor is the largest source of uncertainty and quantifying the delayed particle tail allows for experimenters to reduce said uncertainty [1]. It should be noted that the expected

percent contribution of energy deposition to an experiment package from the delayed particle tail is expected to be larger for pulse reactors than for steady-state reactors due to the nature of the reactor types. For pulse reactors, the delayed particle tail makes up around 10% of the total energy from a pulse [1]. Most often, steady-state reactors are at power for seconds/minutes/hours whereas pulse reactors are "at power" on the order of milliseconds [1].

Because the delayed particle tail of a reactor has yet to be modeled in MCNP with time-dependence, the goal of this paper is to lay out a methodology to model the delayed particle tail produced from a reactor post-shutdown and validate the results with real-world data.

1.2. DIFFICULTIES

The main difficulties with this goal are; (1) MCNP utilizes a static geometry to obtain results, but the pulse/shutdown process is dynamic, (2) the criticality mode within MCNP does not properly simulate delayed particles in time, and (3) the fixed source mode cannot be critical. The following sections will elaborate on these issues further.

1.2.1. Static vs Dynamic Geometry. During a pulse or shutdown, many changes are occurring to a reactor's geometry, namely the withdrawal/insertion of transient/safety/control rods. Unfortunately, MCNP is unable to model this effect properly due to the geometry of a simulation within MCNP being static.

1.2.2. Criticality Mode Improperly Simulating Particles with Time. The criticality mode within MCNP is useful for capturing a source, however it cannot properly simulate delayed particles. When a delayed particle is created within criticality

mode, its "birth time" is set to t = 0, even if the particle is not born at t = 0. While the simplification is necessary for the criticality batching process, it does not simulate the delayed particle population correctly through time. It should also be noted that in MCNP6.2, "delayed-gamma emission is limited to fixed source (SDEF) problems" [3].

1.2.3. Fixed Source Mode Unable to be Critical. The fixed source mode must be used with this problem due to issues with modeling delayed particles in criticality mode. However, the fixed source mode cannot be used for a geometry which is at criticality. This is due to how a "history" is defined within MCNP. In MCNP, the user defines the number of histories (neutron source particles) to be run in a simulation. In criticality mode, this is not a problem as every time a history causes fission, the history's life is ended, and the next history begins. In fixed source mode, a history is effectively "reset" once a particle causes fission. Thus, when a system is in a critical state, a history will generally keep causing fission infinitely and thus the history will generally be reset indefinitely. This leads to a never-ending simulation. To ensure this effect does not occur, the system must be in a state which is subcritical enough to the point that no infinite chains will occur. Figure 1.3 illustrates the difference between a criticality history and a fixed source history.

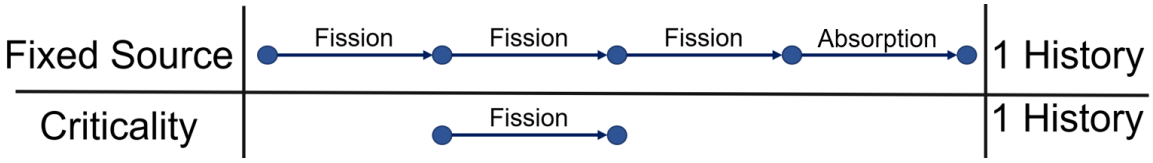

Figure 1.3 Comparison Between Fixed Source and Criticality Modes

2. BACKGROUND

2.1. MCNP DELAYED-PARTICLE MODELING HISTORY

The impact of delayed particles is apparent in subfields of nuclear engineering such as medical physics, experiment package energy deposition, reactor accident scenarios, radiation shielding, etc. [4]. Because of this, in 2005, MCNPX 2.6.0 received delayed neutron and delayed gamma modeling capabilities [4]. These capabilities allowed to user to model delayed particles produced from spontaneous fission, activation, and unstable fission fragments [4]. MNCPX 2.6.0 accomplished this by utilizing a delayed neutron data library containing bin-wise delayed neutron data which was under development since 2004 [5].

In 2010, MCNP6 released with the second release of the delayed library which added support for delayed betas [5]. The third version of the delayed library was never publicly released [5].

In 2014, MCNP6.1.1 released with the fourth version of the delayed library which added support for delayed alphas [5]. The fifth version of the delayed library upgraded the decay data to ENDF/B-VII.1 cross sections, added support for delayed-positrons [4], significantly improved the bin resolution for delayed gammas, and increased the amount of nuclide cross sections available for delayed neutrons, betas, and alphas [5].

In 2017, MCNP6.2 released with the sixth version of the delayed library [3]. This version of MCNP also came with a significant improvement to the line sampling algorithm for delayed gammas [6]. This improvement allowed for delayed gamma line

emission energy sampling to be exact instead of pseudo-random through the utilization of a cumulative distribution function instead of refined bins [6].

2.2. MCNP DELAYED-PARTICLE MODELING THEORY

A delayed-particle physics package requires 4 parts [7]. These components are listed below [7].

1. Precursor sampling
2. Decay-chain methodology
3. Decay data
4. Sampling algorithm

The following sections will further detail these components.

2.2.1. Precursor Sampling. There are two types of neutron precursor sampling physics within MCNP, library-based and model-based [7]. Gamma precursor sampling is limited to only model-based physics [8]. Library physics is typically used at energies under 100 MeV while model physics are used at energies higher than 100 MeV [7]. See Reference 8 for more information on the MCNP delayed neutron and delayed gamma emission data techniques.

Library-based physics is physics based on data files containing cross sections, lists of reactions, distributions, etc. [7]. This type of physics does not compute or provide information about the transmuted nuclei, and residual distributions were left out of libraries due to lack of interest [7]. The major disadvantage of this method is it utilizes a six-time group approximation for residuals [8]. Figure 2.1 shows the procedure for producing delayed neutrons for neutron-induced fission reactions using the library-data

technique. See Reference 8 for more information on the delayed neutron library-based physics procedure.

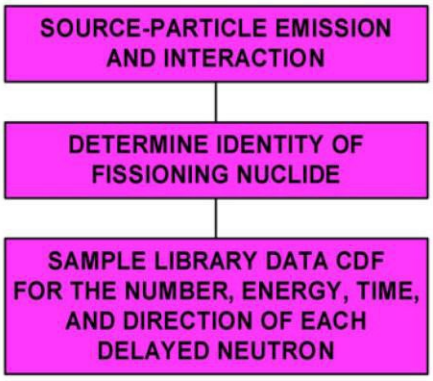

Figure 2.1 MCNP6 Delayed Neutron Production From Fission Reactions Procedure Using Library-Based Technique [8]

On the other hand, model-based physics "can be used to produce delayed neutrons for fission or activation events induced by any source particle treated by MCNP" and is the sole method for producing delayed gammas within MCNP [8]. Model-based physics also provides accurate identification of residuals, preserving isotopic time dependence [7, 8]. Due to the lack of residual distributions, high-fidelity fission-product distributions are used for fission reactions and a conversion algorithm is utilized for non-fission reactions in MCNP6 for neutrons [7]. This conversion algorithm creates a table listing all library reactions and their related nucleonic adjustments [7]. England and Rider developed neutron-induced fission yield sets for thermal, fast, and high energy regimes used by MCNP6 [7]. The General Description of Fission Observables (GEF) code is utilized by MCNP6 for photon-induced fission yields [7]. For more information regarding the England and Rider yield sets or the GEF code, refer to References 9 and 10, respectively.

Figure 2.2 shows the procedure for producing delayed neutrons/gammas for fission and activation reactions using model-based physics. See Reference 8 for more information on the delayed neutron/gamma model-based physics procedure.

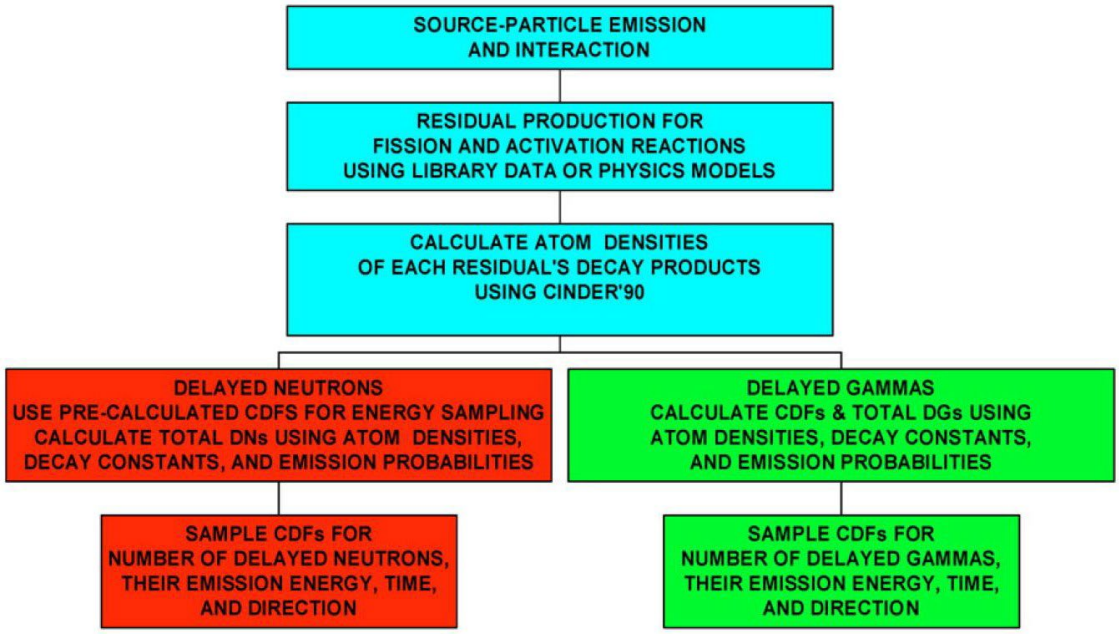

Figure 2.2 MCNP6 Delayed Neutron/Gamma Production From Fission and Activation Reactions Procedure Using Model-Based Technique [8]

2.2.2. Decay-Chain Methodology. Within MCNP6, CINDER90 allows for quick decay-chain isotopic calculations [7]. Reference 11 explains the decay-chain isotopic in greater depth. This function provides the delayed-particle physics package isotopic emission probabilities [7]. Reference 12 provides more details about the isotopic emission probabilities.

2.2.3. Decay Data. A Compact ENDF (ACE) file data is utilized to calculate particle emission when library-based physics is enabled for delayed neutrons from fission

interactions [3]. DELAY_LIBRARY_V5.dat library data is used when the model-based physics is enabled for delayed neutrons from fission and/or non-fission interactions [3]. ENDF/B-VII.1 line emission data within CINDERGL.dat augmented by DELAY_LIBRARY_V5.dat model data is utilized to calculate delayed gamma emission [3]. The DELAY_LIBRARY_V5.dat data is the only source of sampling for delayed betas, alphas, and positrons [3]. Specific radionuclide delayed particle spectra are stored within the DELAY_LIBRARY_V5.dat library for neutrons, gammas, betas, alphas, and positrons [3].

2.2.4. Sampling Algorithm. There are two types of sampling algorithms within MCNP6, bin- and line-based [7]. Line-based sampling is more exact but is far slower than bin-based sampling. References 8 and 12 contain more information on these algorithm types.

2.3. VALIDATING MCNP DELAYED PARTICLE MODELING ACCURACY

Many tests have been performed utilizing MCNP delayed particle modeling to attempt new implementations of the modeling capability and benchmark the modeling results with measured values from experiments. The following sections will discuss tests done with MCNP delayed particle modeling.

2.3.1. Method for Calculating Delayed Gamma-Ray Response in the ACRR Central Cavity and FREC-II Cavity Using MCNP. This paper from Sandia National Laboratory (SNL) focuses on the methodology created to characterize "delayed gamma-ray radiation fields in pulse reactors like the Annular Core Research Reactor (ACRR) and the Fueled Ring External Cavity (FREC-II)" [13]. This paper focuses on

creating a source distribution from the MCNP KCODE (criticality mode) source tapes then applying delayed particle physics to characterize the delayed gamma-ray radiation fields [13]. The results obtained using this methodology agreed well with real data [13]. This paper displays the ability to capture a reactor as a source in criticality mode using source tapes and use the source created in a fixed source calculation to quantify the impact of delayed gammas.

2.3.2. Simulation of Delayed Gamma Rays from Neutron-Induced Fissions Using MCNP 6.1. This study looked at the delayed gamma rays emitted from neutron-activated uranium and plutonium samples which were irradiated for 2 hours with a pulsed deuterium-tritium (D-T) neutron generator [14]. The activated samples were placed in a gamma spectroscopy station to find the time dependent delayed gamma flux distribution [14]. The study noted the MCNP simulated net gamma counts matched the experimental values from the uranium and plutonium samples, but the decay curves showed non-physical discontinuities [14]. The experiment was repeated for copper and aluminum and the non-physical discontinuities in the time-dependent gamma flux distribution were no longer found and the half-lives of the data matched that of the expected activated copper/aluminum isotopes [14]. This study shows the MCNP 6.1 delayed gamma modeling capabilities may result in unexpected discontinuities. These discontinuities may be caused by the pseudo-random nature of the delayed gamma line sampling method. However, this is only stipulation as the paper did not specify the delayed gamma emission method used within MCNP on the activation (ACT) card.

2.3.3. Delayed Gamma Radiation Simulation in Case of Loss of Water Event Using Monte Carlo Method. This analysis investigated the dose rates created during a

loss of water event [15]. The MCNP results were validated by measuring the dose rates of irradiated Training, Research, Isotopes, General Atomics (TRIGA) fuel in a transport cask [15]. The measurements were compared to MCNP dose rate results with delayed gammas enabled and were found to be in agreement [15]. This validation provides confidence the delayed gamma capability in MCNP provides correct answers even when dealing with more complicated sources such as TRIGA fuel.

2.3.4. Simulation of Delayed Neutrons Using MCNP. This study first compares MCNP delayed neutron relative power results to the results from the impulse response function and found the results to be in agreement [16]. Both MCNP and analytical solution utilized a ^{235}U 8.5407 cm radius sphere and 50 million source neutrons were ran in the MCNP simulation [16]. An experiment was then performed on the Westinghouse Idaho Nuclear Company (WINCO) Slab Tank Assembly [16]. This experiment placed a californium source between two uranyl-nitrate cylinders [16]. The cylinders were brought together until source equilibrium was achieved [16]. At this point, the source was rapidly removed, and neutron intensity was measured as a function of time [16]. This experiment was replicated in MCNP and obtained results which matched well with the experiment [16]. This study provides confidence in the ability to model delayed neutrons within MCNP and utilized two methods (analytical and experimental) to prove it.

2.3.5. Calculating the Effective Delayed Neutron Fraction with Monte Carlo. This study utilized MCNP to calculate the effective delayed neutron fraction (β_{eff}) of many benchmark experiments [17]. The study compared multiple methods for calculating β_{eff} and attempted to quantify how different sources of nuclear cross sections impacted the results [17]. The study generally found success with calculating β_{eff}, often the

calculated value only deviated from the measured value by around 5% for the 8 benchmark experiments tested [17]. The study could not find a relationship between different nuclear data sources and their impact on β_{eff} [17]. This study implies that the delayed neutron modeling capabilities within MCNP are adequate and can be utilized on benchmark systems instead of simple sources.

2.3.6. A Preliminary Comparison of MCNP6 Delayed Neutron Emission from ^{235}U and Experimental Measurements. This study involved irradiating a ^{235}U solution then counting the delayed neutron count rate over 3 minutes utilizing ^{3}He detectors [18]. The setup was then modeled within MCNP, and the time-dependent neutron count rate was compared between the experiment and MCNP results [18]. The MCNP results were repeated, once with the delayed neutron bias (dnb) option in the neutron physics (PHYS:N) card set to ACE, and another with the dnb option set to CINDER [18]. The experiment found that both MCNP results generally agree with the experimental data [18]. The MCNP results utilizing the ACE dnb option matched the experiment results better at later time bins while the MCNP results utilizing the CINDER dnb option matched the experiment results better at early time bins [18]. The CINDER MCNP results overestimated the experimental delayed neutron count rate and altered in behavior from experimental results after about 2 minutes [18]. This study displays the ability of MCNP to model the delayed neutron emission of irradiated fissile material.

3. METHODOLOGY

To solve the difficulties brought up in Section 1.2, the methodology outlined below will be utilized. This methodology is similar to that discussed in Section 2.3.1; however, a different method will be utilized to capture the source and this paper focuses on capturing the time-dependent delayed particle tail of a reactor as opposed to characterizing delayed gamma radiation fields. Figure 3.1 outlines the methodology.

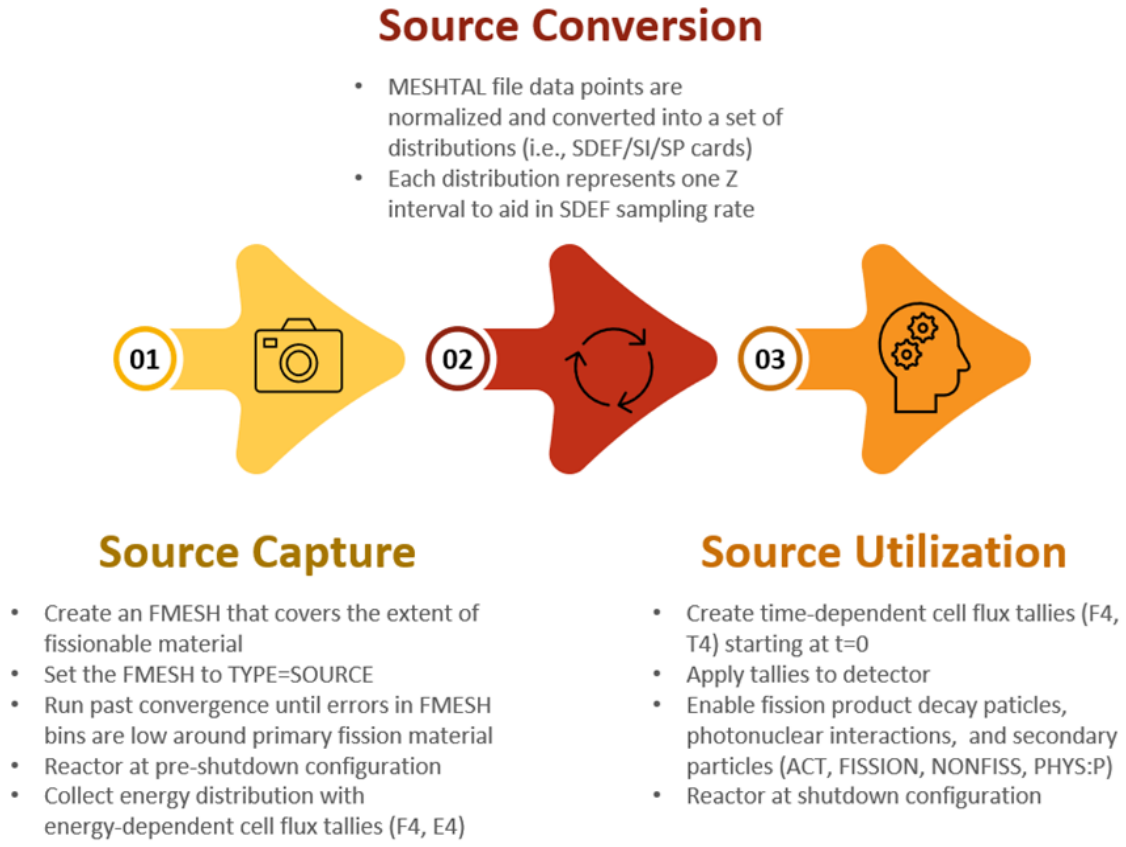

Figure 3.1 Methodology Outline

The following sections will explain each step more in-depth.

3.1. SOURCE CREATION

The source should be captured in MCNP at either the pulse configuration (for pulse reactors) or steady state critical configuration (for steady state reactors) because these configurations are where most of the delayed-particle-producing particles will be born. The two main ways to accomplish this in MCNP is by utilizing Surface Source Write/Read (SSW/SSR) and FMESH. Table 3.1 summarizes the advantages and disadvantages of each method.

Table 3.1 SSW/SSR Comparison to FMESH [1]

	SSW/SSR	FMESH
Advantages	- Easier to implement. - Captures weight, energy, and neutrons per fission from each site.	- No particle limits in fixed source mode. - Greater control over source information collection. - Captures the true converged source distribution limited by stochastic sampling instead of number of particles run.
Disadvantages	- Large source file (~10-100s GB). - Fixed source particle history weight limited to number of particles run in criticality mode for SSW/SSR capture. - Not compatible with “tasks” command.	- Fission source distribution not exact due to integration over a voxel. - Must recreate the source externally to MCNP. - Large SDEF distribution slows transport.

SSW/SSR is easier to implement compared to FMESH. An SSW card is implemented into a criticality run and the source is captured and ready to be used in an output file with an SSR card. No post-processing is required. SSW also captures more information from each source site including particle weight and energy. However, capturing so much information creates a large source file (~10-100s GB). Uploading or moving this file anywhere takes long periods of time. SSW/SSR also requires weight normalizations between runs with varying particle histories. If 100 particles with a weight of 1 were used to create an SSR input file, and the user wanted to use this source and run 200 particles, the weight of each particle would be halved to conserve the total weight between runs. There is an option to multiply the weight to avoid this normalization, but it must be calculated and implemented between every run which is an annoyance. SSW/SSR is also inapplicable with the tasks command. Message Passing Interface (MPI) tasks could be utilized, but this process is difficult on a personal computer and the SSW file can exceed the memory on a particular node, causing the node to crash on a high-performance computing (HPC) machine.

FMESH does not require particle weight normalizations between runs with various histories. If 100 particles with a weight of 1 were used to capture the source, and the user wanted to use this source and run 200 particles, the weight of each particle would remain one as total weight need not be conserved between runs as in SSW/SSR. FMESH also gives the user greater control over the source information collected. The user can make the FMESH voxels as fine or as coarse as desired. However, the source distribution introduces error as the result is averaged over a voxel. This error is not expected to impact results once enough voxels are utilized to capture the source as it is expected the

error will average out. However, the FMESH output MESHTAL file must be post-processed before using the results as a source definition. The energy distribution within the system must then be found and implemented into the source definition. And finally, the complicated source definition slows transport. SSW/SSR has the data written to its file and has no need for position or energy sampling, but the FMESH requires MCNP to decide the position and energy based off a probability distribution.

Although SSW/SSR is easier to implement and captures more information from a source site than FMESH, the flexibility FMESH allows by giving the user greater source fidelity control as well as a far smaller source file storage size is invaluable. Thus, FMESH was chosen as the method to capture the reactor as a source.

"The FMESH card allows the user to define a mesh tally superimposed over the problem geometry. Results are written to a separate output file with the default name MESHTAL. By default, the mesh tally calculates the track length estimate of the particle flux averaged over a mesh cell in units of particles/cm^2" [3]. There are multiple types of tallies within MCNP and each tally records different information from the problem. See Section 1.3.4.4 of Reference 3 for more details on the types of tallies and how the tally information is calculated. The track-length estimate methodology will be further explained in the F4 tally paragraph of this section.

Form: FMESHn:<pl> KEYWORD = value(s) [3]

"Where n is a tally number ending in the numeral 4 (only type 4 volume flux tallies are permitted) and <pl> = N, P, or E" [3].

For example, take the following FMESH:

FMESH4:N ORIGIN = -10 -10 -10 IMESH = 10 JMESH = 10 KMESH = 10

IINTS = 3 JINTS = 3 KINTS = 3 TYPE = SOURCE

The example FMESH would create a 20x20x20 cm mesh cube with its center at (0,0,0). 27 smaller similar cube voxels would be contained in the 20x20x20cm mesh cube, and the FMESH tally would record neutron source points within each of the 27 voxels. Figure 3.2 shows a visual representation of the FMESH from the above example. The geometry is shown in red, yellow, and blue and the superimposed mesh voxels are indicated by the blue squares. The user would be able to find flux, reaction rates, heating, etc. in each of these voxels.

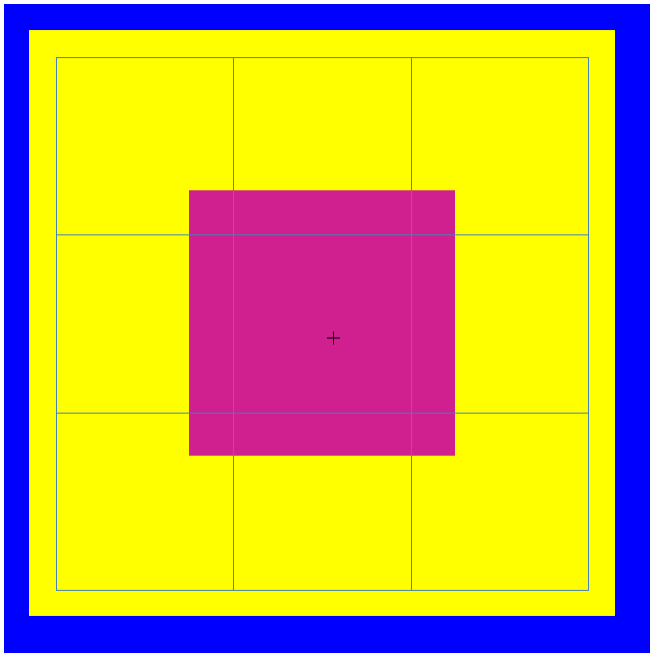

Figure 3.2 FMESH Geometry and Mesh Example

The most important option for this methodology is the TYPE option. If the user sets the TYPE to SOURCE for an FMESH, the user obtains the distribution of the source

points in the FMESH. The user must ensure the average error in the voxels is acceptable as high errors means the MESHTAL file does not accurately simulate the source distribution. This FMESH superimposed mesh can be as fine or coarse as the user desires. More voxels means the source distribution more closely resembles the actual reactor source, but it takes longer to create (as more particles are required to obtain acceptable MESHTAL errors and the source conversion process will take longer) and slows source sampling during runs due to a more complicated SDEF. In general, a parameterization study should be conducted to identify the optimal FMESH fidelity for the reactor. For more information on FMESH, refer to Section 3.3.5.25 of Reference 3.

To find the energy distribution of the source, an F4 tally was utilized. The F4 tally is the track-length estimate of cell flux [3]. The track-length estimate for flux assumes the relative flux in a cell is directly proportional to the total distance of all particles (of a user-specified type) traveled within the cell of interest.

Form: Fn:<pl> $s_i \ldots s_k$ [3]

For example, take the following tally: F14:N 1000 1001

This tally is a cell flux tally with tally number 14. The particle for which flux is being calculated is neutrons. The cell numbers for which neutron flux is being calculated is 1000 and 1001. Table 3.2 below shows the equation for the score and physical quantity, as well as the units of the F4 tally. The score equation in Table 3.2 assumes all particles contributing to the F4 tally are the same weight and travel the same distance within the F4 cell. Table 3.3 describes the parameters within the equation for score. Equation (1) shows the formula to calculate the F4 tally result when particles are at varying weights and travel various distances throughout the F4 cell.

Table 3.2 Score, Physical Quantity, and Units for F4 Tally [3]

Score (Result)	Physical Quantity	Units
$W\frac{T_l}{V}$	$\bar{\phi}_V = \frac{1}{V}\int dE \int dt \int dV \int d\Omega\ \psi(\vec{r}, \Omega, E, t)$	particles/cm^2

Table 3.3 Score Parameter Descriptions [3]

Parameter	Description
W	Particle weight
T_l	Track length (cm) = event transient time x particle velocity
V	Cell volume (cm^3) calculated by the code or input by the user

$$\emptyset = \frac{1}{V * W} \sum_{all\ flights\ in\ cell} wgt * dist \quad (1)$$

Where V = cell volume [cm^3]

W = total source weight

wgt = individual particle weight

$dist$ = individual particle travel distance through cell [cm]

The particle weight is a multiplier applied to the total score of a given particle. Higher weight particles carry a larger impact on tally results. The score of a tally is simply the result of the tally. Normally many high-weight particles contributing to the tally of interest is desired as it means fewer total particles must be run. The F4 tally

utilizes a track-length estimate to calculate flux. The track-length of a particle is the distance a particle travels through a cell. Once the total track-length is found, the result is then normalized by the cell volume. This method provides a reasonable estimate of the particle flux within a cell.

Figure 3.3 shows an example of particle transport within MCNP.

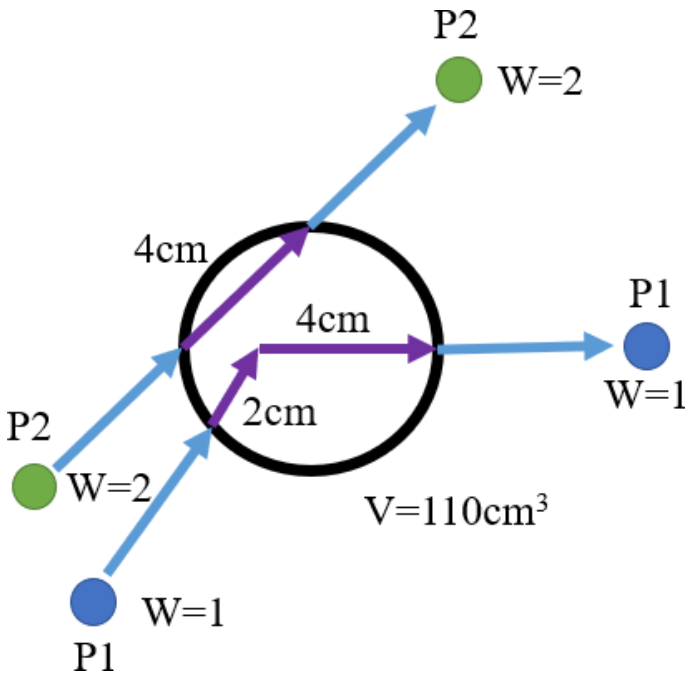

Figure 3.3 F4 Tally Calculation Example

Here, 2 particles enter and exit the cell of interest. These two particles are the only particles modeled within the simulation. The weight of particle P1 is one and the weight of particle P2 is two. The volume of the cell is 110 cubic centimeters. Particle P2 traveled a total of six centimeters through the cell and particle P2 traveled a total of four centimeters through the cell. Using Equation (1), the track-length estimate of cell flux can be calculated.

$$\emptyset = \frac{1}{V * W} \sum_{all\ flights\ in\ cell} wgt * dist = \frac{1}{110 * (1+2)}(1 * 6 + 2 * 4) = 4.24E-2$$

The units of this track-length estimate of cell flux are in #/cm^2. To convert this output to appropriate units of flux (neutrons/cm^2*s), this value would be multiplied by the number of neutrons per second being emitted by the source of neutrons. See Section 3.3.5.1.1 of Reference 3 for more information about the F4 tally.

To split the flux into an energy-dependent flux distribution, the En card was utilized.

Form: En $e_1 \ldots e_k$ [NT] [C] [3]

For example, take the following tally energy card:

E14 1 2 3 4 5

This tally energy card would split up the F14 cell flux tally results into 5 equally spaced 1 MeV wide energy bins.

3.2. SOURCE CONVERSION

The MESHTAL file will contain the midpoint X, Y, and Z values, result, and relative error of each FMESH voxel. All these values were first copied to an Excel file and the voxels with a result of 0 were removed. Then, the voxels were organized from lowest-to-highest Z values. The total results for each horizontal slice of the FMESH were found and normalized against the total result for the entire FMESH. This creates a Z-distribution within the source definition and greatly increases the source sampling speed. After this, each (X, Y) point in a Z-slice had its results normalized against the total

Z-slice results to create a source distribution within each Z-slice. The F4 tally individual energy bin results were normalized against the total F4 result to create an energy distribution within the source distribution. The energy and Z-slice distributions were implemented into a single SDEF file utilizing SDEF/SI/SP cards.

3.3. SOURCE UTILIZATION

The SDEF file from the end of Section 3.2 is then read into the input file using the READ card in MCNP. Once read into the input file, appropriate tallies and physics are implemented into the shutdown geometry configuration input file to obtain the delayed particle tail in MCNP. These tallies and physics are discussed further in the following sections.

3.3.1. Tallies. To obtain the time-dependent delayed-particle tail within MCNP, an F4 tally was used in tandem with a time cell flux (T4) card. The detector which measures reactor power is the cell which the user should tally. A cell in MCNP is a user-defined space defined by Boolean algebra utilizing user-defined surfaces. See Section 3.2.2 of Reference 3 for a comprehensive list of available surfaces. Two F4 tallies should be made, one for photons (<pl> = p) and one for neutrons (<pl> = n). This will provide the user with photon and neutron flux which are the primary particles contributing to decay heat.

Along with the F4 tally, T4 cards are required. The T4 card splits the F4 tally into energy bins so the user can obtain bin-wise time-dependent particle flux.

Form: Tn $t_1 \ldots t_k$ [3]

For example, take the following time card:

T14 1E8 2E8 3E8

This time card would create three time bins from 0 shakes to 1E8 shakes, 1E8 shakes to 2E8 shakes, and finally from 2E8 shakes to 3E8 shakes. This is equivalent to time bins from 0 to 3 seconds in steps of 1 second. These time bins would be created for tally number 14, meaning that this time bin would properly split the F14 tally used earlier in the example.

The size and frequency of the time bins depends on the problem being solved. It should be noted that it becomes increasingly difficult to have particles score on a specified tally at later time bins since less particles are present at later times in a MCNP simulation. Thus, in general the time width of a time bin should be increased as the time bins go further in time. Increasing the time width of a time bin increases the probability of a particle contributing to it. Thus, better statistics can be obtained while running the same number of particles at the cost of result fidelity.

3.3.2. Physics. The main physics within this MCNP problem which deviate from normal is the presence of delayed particles, photons, model physics, and photonuclear particle production. The following paragraphs will explain these physics further.

First, delayed particles must be enabled in MCNP. The user accomplishes this with the ACT card built into MCNP6.2.

Form: ACT KEYWORD = value(s) [3]

For example, take the following activation card:

ACT FISSION = N NONFISS=P DN = MODEL DG = LINES DNBIAS = 1

This activation card would produce delayed neutrons from fission residuals and delayed gammas from non-fission reactions. The delayed neutrons would be produced from models and the delayed gammas would be produced using models based upon

line-emission data augmented by the delay_library_v[n].dat data. Finally, one delayed neutron would be produced per delayed neutron interaction.

Photon transport must be enabled within the MCNP simulation. This is accomplished utilizing the MODE card in MCNP. “By default, MODE N P does not account for photo-neutrons but does account for neutron-induced photons. Photonuclear particle production must be turned on utilizing the photon physics (PHYS:P) card” [3].

For example, take the following MODE card:

MODE N P

This MODE card would enable photon and neutron transport within the simulation.

As mentioned before, photonuclear particle production must be enabled using the PHYS:P card within MCNP. The user is given the option between analog and biased photonuclear particle production.

Form: PHYS:P emcpf ides nocoh ispn nodop J fism [3]

For example, take the following photon physics card:

PHYS:P 3J -1

This card would enable analog photonuclear particle production within the problem.

Due to missing photonuclear interaction cross-sections for certain isotopes within MCNP, the nuclide substitution (MXm) card was required. “The parameter ‘0’ on an MXm card eliminates all interaction physics, whether model or table-based.” [3].

Form: MXm:<pl> $zaid_1$ $zaid_2$… [3]

For example, take the following nuclide substitution card:

MX3:P J 0 0 J

This nuclide substitution card would disable photonuclear cross sections for the second and third isotope specified in the third material (M3) card. See Reference 3 for more information regarding the Mm card.

The user utilizes the NPS card to specify the number of particle histories to simulate.

Form: NPS npp npsmg [3]

For example, take the following history cutoff card:

NPS 1E7

This NPS card would stop the simulation after 1E7 particles were simulated.

The model physics (MPHYS) card within MCNP controls the use of physics models. Since delayed particles utilize model physics for emission calculations in MCNP, this card will be required.

Form: MPHYS [ON/OFF] [3]

For example, take the following model physics control card:

MPHYS ON

This card would enable model physics for the simulation.

3.3.3. Variance Reduction. The goal of variance reduction is to increase the figure of merit (FOM) of the tally of interest while retaining accuracy. The equation for calculating the figure of merit is shown in Equation (2) [3].

$$FOM = \frac{1}{\sigma 2t} \tag{2}$$

Where σ = the tally relative error and

t = computer run-time

Thus, if the computer run-time can be reduced while obtaining the same statistics (similar tally relative error), then the FOM will increase and the simulation is more efficient. However, the accuracy of the tally results should be verified to ensure the variance reduction techniques are not resulting in incorrect answers.

The main methods for variance reduction applicable to this methodology include weight window generator (WWG), time splitting (TSPLT), and the time cutting (CUT). The following sections will explain how these methods assist in achieving more efficient statistics. It should be noted that deterministic transport (DXTRAN) spheres were investigated for this problem but were found to decrease the FOM of the simulation.

3.3.3.1. Weight window generator (WWG). "The WWG card allows the code to generate an importance function for a user-specified tally" [3]. "For the mesh-based weight window generator, the code writes the weight-window lower bounds and a mesh description only to the WWOUT file" [3]. "[T]he generated weight-window information can be easily used in subsequent runs using switch < 0 on the WWP card. For many problems, the weight-window generator results are superior to anything an experienced user can guess and then input on an IMP card" [3].

Form: WWG i_t i_c w_g J J J J i_E [3]

For example, take the following weight window generator card:

WWG 14 0 0 J J J J 0

This weight window generator would optimize the weight windows for tally 14, invoke mesh-based weight windows (meaning a MESH card would be required), set the lower bound to be half the average source weight (recommended in most cases), and interpret WWGE card entries as energy bins.

The MESH card sets the superimposed importance mesh for the mesh-based weight-window generator.

Form: MESH KEYWORD = value(s)… [3]

For example, take the following weight window generator MESH card:

MESH GEOM = XYZ ORIGIN = -5 -5 -5 IMESH = 5 JMESH = 5

KMESH = 5 REF = 0 0 0 IINTS = 2 JINTS = 2 KINTS = 2

This mesh would be a cube mesh with its center at (0,0,0) with side lengths of 10cm. Each side would be split in half resulting in 8 5x5x5cm voxels being created. The WWG card would then create a WWOUT file with weights for each of these voxels. The weight for each voxel would try to maximize the number and weight of particles which may contribute to the tally specified in the WWG card. The reference point should be a point in fueled material so it is implied that fuel resides at (0,0,0).

To utilize a WWOUT file created from a weight window generator run, the weight-window parameter (WWP) card must be utilized. “The WWP card contains parameters that control various aspects of the weight-window game” [3].

Form: WWP:<pl> wupn wsurvn mxspln mwhere switchn mtime wnorm etsplt wu [3]

For example, take the following weight window parameter card:

WWP:N 4J -1 2J 1

This card would enable mesh-based weight window inputs for neutrons and would cause the TSPLT card to roulette particles in addition to scaling the weight windows.

Since mesh-based weight windows are to be used from a WWOUT file, switchn is to be set to -1. When running the file in command line, “WWINP=WWOUT_FileName” must be added to utilize the WWOUT file created from the WWG run. Also, since TSPLT is recommended, etsplt should be set to 1 so that the TSPLT can be used to roulette particles. TSPLT will be further discussed in the next section.

3.3.3.2. Time splitting (TSPLT). “The TSPLT card allows problem-wide splitting and Russian roulette or particles in time, like the IMP card allows splitting and Russian roulette as a function of geometry… The changes to a particle’s weight caused by the TSPLT card will create compensating weight adjustments to the weight cutoff and weight-window values” [3].

For example, take the following time split card:

TSPLT:N 2 1E8 4 2E8 8 3E8 16 4E8

This card would cause neutrons to split exponentially in the first 4 seconds of the problem time. Neutrons which are alive at 1E8 shakes would be split in half and each particle would have half of their original weight. Then the particles alive at 2E8, 3E8, and 4E8 shakes would be split by 4, 8, and 16 times, respectively.

Form: TSPLT:<pl> r_1 t_1 … r_{20} t_{20} [3]

TSPLT assists in this methodology as it can split particles at the later time bins. This artificially increases the number of particles at a given time (although weight remains conserved) which increases the likelihood of contributions to the tally at a certain time bin. Because particles exponentially decay with time, a tiered, exponential TSPLT would likely result in the most efficient calculation.

3.3.3.3. Time cutting (CUT). The CUT card is a physics cutoff card which can change the maximum time for which delayed particle emission is calculated.

Form: CUT:<pl> t e wc_1 wc_2 swtm [3]

For example, take the following time split card:

CUT:N 3E9

This card would cutoff delayed particle emission calculations at 3E9 shakes. This card is useful as the default times for neutrons and photons is very large. Utilizing the CUT card avoids unnecessary delayed particle modeling which would not be able to contribute to a time bin since the particle is alive after the latest time bin cutoff.

4. METHODOLOGY APPLICATION

To validate the methodology, real world data was acquired from the Missouri S&T Reactor (MSTR). This data is from a compensating ion chamber (CIC). Figure 4.1 shows the Missouri S&T Reactor.

Figure 4.1 Missouri S&T Reactor (MSTR)

The MSTR was chosen because high-fidelity full-power time-dependent SCRAM data was readily available and because the reactor was easily accessible to the author should any measurements need to be taken. The SCRAM data went out to about 30 minutes post-shutdown. The MSTR is a 200kW open-pool type reactor with materials

test reactor (MTR) type fuel. The fuel meat is U_3Si_2 enriched to about 20% ^{235}U. The core is cooled by the natural convection of water and a MCNP6.2 model was readily available.

Figures 4.2 and 4.3 show the horizontal and axial MCNP cross sections of the MSTR, respectfully. The blue squares within the Figures show the mesh voxels used for the source capture FMESH. The curved fuel plates within the fuel can be clearly seen. A fuel assembly is outlined in orange. The control rods elements are outlined in yellow. The core access element (CAE) is outlined in gray. The element which holds the PuBe neutron startup source is outlined in blue. The three pneumatic tube experimental facilities are outlined in purple. The center element is the irradiation fuel element. The top-right element position in the model is vacant.

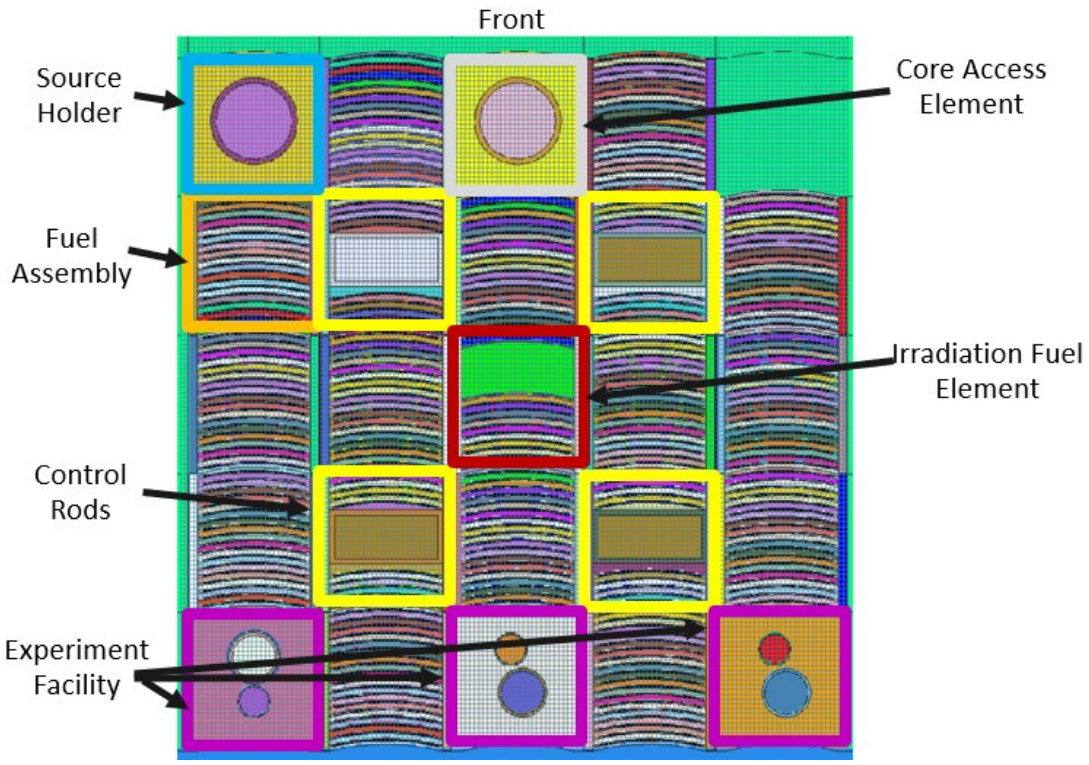

Figure 4.2 Horizontal Cross Section of MSTR

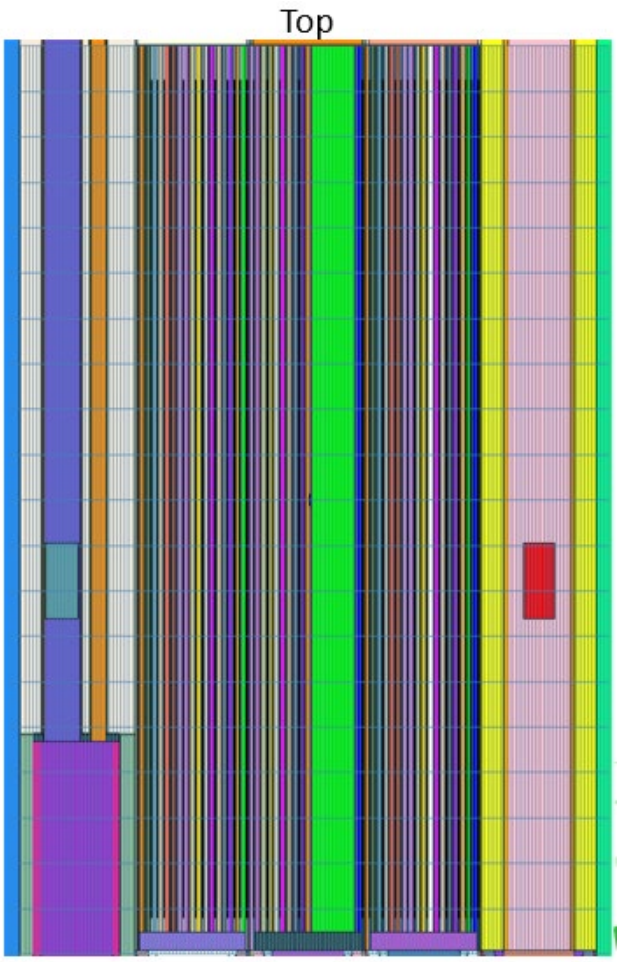

Figure 4.3 Axial Cross Section of MSTR

Figures 4.4 and 4.5 compare the lateral MSTR cross section of reality versus the MCNP model, respectively. The difference between the Figures displays the simplifications made in the MCNP model. Namely the lack of bridge assembly, tower assembly thermal column door assembly, fuel element storage rack, and detector guide assemblies. The concrete beyond the water and behind the thermal column is also missing from the MCNP model.

It should be noted that room temperature ENDF/B-VIII.0 nuclear data libraries were used for all results obtained [19].

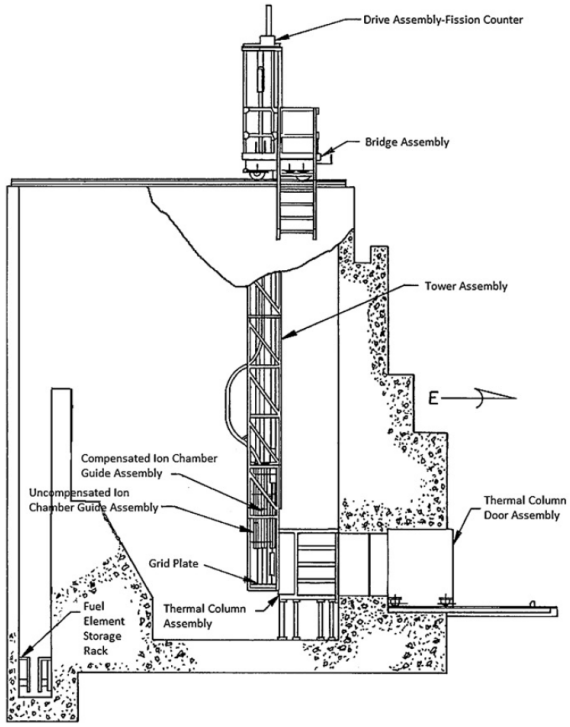

Figure 4.4 MSTR Design Lateral Cross Section [20]

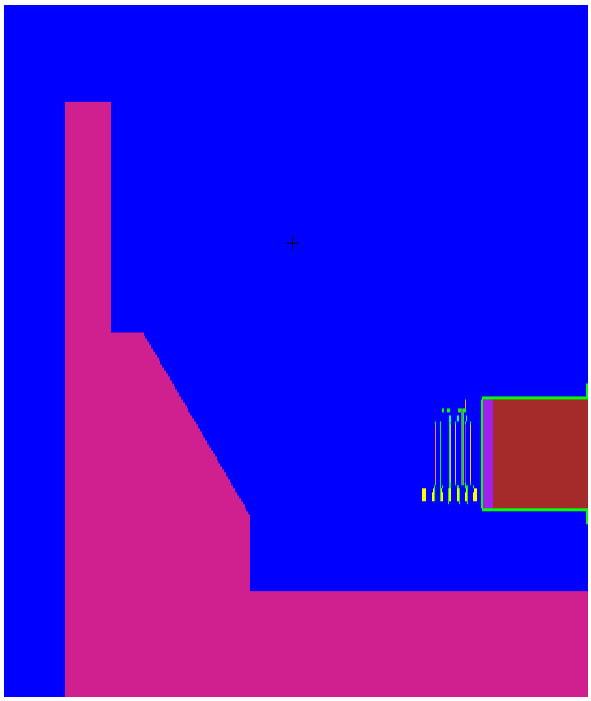

Figure 4.5 MCNP Model Lateral Cross Section

MSTR burnup values are not exact for each fuel element due to the volatile power history of the MSTR. This volatile power history is a product of the reactor being used purely for research, classwork, and training. The MSTR rarely stays at power for longer than a few hours as often it is being used by trainees to practice power changes for licensing requirements. Thus, there is some uncertainty in the material cards regarding the fuel, although this impact is expected to be negligible due to the low overall burnup of the MSTR. The fuel materials have been updated for the current on-record burnup.

4.1. SOURCE CREATION

To create the MSTR source, an FMESH with TYPE = SOURCE was created which covered the fuel within the MCNP model while the model was at critical. Figure 4.6 shows the FMESH card used to create the source definition for the MSTR. The 150x150x20 superimposed mesh can be seen visually by the blue lines in Figures 4.2 and 4.3. This means the FMESH has 450,000 voxels each 0.26x0.28x3.2 cubic centimeters in size to represent the source distribution. This many source points means the source should accurately simulate the reactor if the relative errors of the voxels are acceptable. This many source points also means the error created by the integration over an FMESH voxel should be negligible. It is likely that this many source points is far higher than is required to accurately capture the source. Therefore, a parameterization study should be conducted to identify the optimal FMESH size for the reactor. This would avoid over-capturing the reactor which leads to an overly-complicated source distribution which increases run-time. However, a source parametrization study was beyond the scope of this work and was thus not performed.

```
FMESH4:n ORIGIN=-12 -25 -32 TYPE=SOURCE
         IMESH=27 IINTS=150
         JMESH=17 JINTS=150
         KMESH=32 KINTS=20
```

Figure 4.6 FMESH Parameters for MSTR SDEF

Figures 4.7 and 4.8 show the FMESH MESHTAL visual results for the horizontal and axial cross sections, respectively (red denotes a higher concentration of source particles and blue denotes a lower concentration of source particles). This MESHTAL output represents the source distribution within the reactor. These figures match common knowledge of the MSTR because the MESHTAL output (neutron source point intensity) peaks at the center of the reactor and decreases at the edges of the reactor as expected. The MESHTAL also obtains results only in voxels containing fissile materials which is expected as there would be no neutron source points within the water as no fission is occurring in the water. The voxel errors in this MESHTAL were below 5% on average which was deemed acceptable to move on. See Appendix A for the partial MSTR MESHTAL output file.

After the source distribution was obtained, the energy distribution was captured. This involved placing an F4 tally on the CAE. The CAE was chosen to be tallied upon as it is the nearest cavity to the core available in the MCNP model. The F4 tally was split utilizing an 89-energy group structure E card. 89-energy groups were determined to be fine enough to obtain an accurate energy distribution within the reactor. Figure 4.9 shows the F4 tally utilized to obtain the energy distribution. Cell 7425 within the MCNP model is the CAE. The errors obtained in the results were below 2% on average.

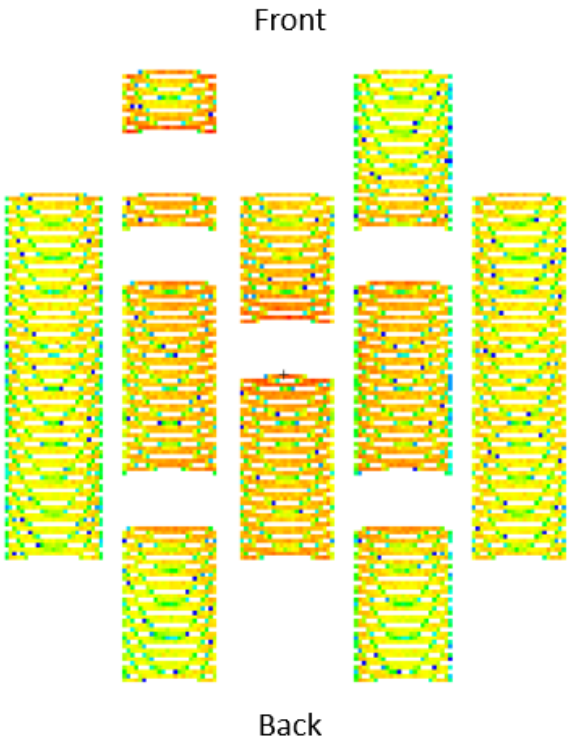

Figure 4.7 FMESH Results for Horizontal Cross Section

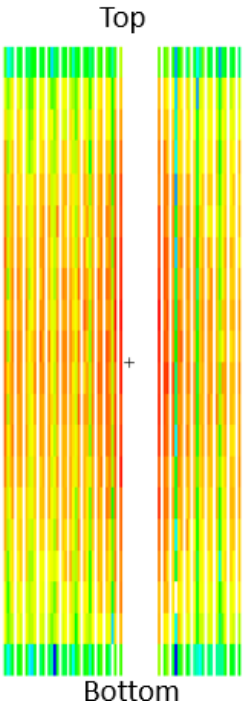

Figure 4.8 FMESH Results for Axial Cross Section

```
F14:N 7425
E14  1.39E-10     1.00E-09     5.00E-09     1.00E-08     3.00E-08
     7.00E-08     1.00E-07     1.52E-07     2.00E-07     4.14E-07
     6.00E-07     8.00E-07     1.13E-06     3.06E-06     5.04E-06
     8.32E-06     1.37E-05     2.26E-05     3.73E-05     6.14E-05
     1.01E-04     1.67E-04     2.75E-04     3.54E-04     4.54E-04
     5.83E-04     7.49E-04     9.61E-04     1.09E-03     1.23E-03
     1.40E-03     1.58E-03     1.80E-03     2.03E-03     2.31E-03
     2.61E-03     2.96E-03     3.35E-03     3.80E-03     4.31E-03
     4.88E-03     5.53E-03     6.27E-03     7.10E-03     8.05E-03
     9.12E-03     1.03E-02     1.17E-02     1.33E-02     1.50E-02
     1.70E-02     1.93E-02     2.19E-02     2.48E-02     2.61E-02
     2.81E-02     3.18E-02     4.09E-02     5.25E-02     6.74E-02
     8.65E-02     1.11E-01     1.43E-01     1.83E-01     2.35E-01
     3.02E-01     3.88E-01     4.39E-01     4.98E-01     5.64E-01
     6.39E-01     7.24E-01     8.21E-01     9.30E-01     1.05E+00
     1.19E+00     1.35E+00     1.74E+00     2.23E+00     2.87E+00
     3.68E+00     4.72E+00     6.07E+00     7.79E+00     1.00E+01
     1.19E+01     1.35E+01     1.49E+01     1.69E+01     2.00E+01
```

Figure 4.9 F4 Energy Bins for MSTR Energy Distribution

4.2. SOURCE CONVERSION

The MESHTAL data and F4 energy distribution results were converted to a SDEF utilizing the methodology laid out in Section 3.2. See Appendix B for the partial MSTR SDEF input file.

4.3. SOURCE UTILIZATION

The READ card in MCNP was used to read-in the SDEF file created in Section 4.2 as seen in Figure 4.10. The NOECHO option was utilized in the READ card to keep the output file clean as the MSTR SDEF file is over 300,000 lines long. This is also why only part of the MSTR SDEF input file was included in Appendix B. The following sections will specify the tallies and physics used for MSTR to obtain the delayed particle tail.

```
READ File=MSTR_SDEF.txt NOECHO
```

Figure 4.10 READ Card Utilized for Input File

4.3.1. Tallies. Because the CIC detector was not modeled in the given MCNP input, the F4 tally was applied to the CAE of the MSTR (refer to Figure 4.2 for CAE location).

45 total time bins were utilized to capture the MSTR delayed particle tail. 20 time bins were applied to the F4 tally from initial shutdown to 5 minutes (0.25 minute time bins). 25 time bins were applied to the F4 tally from 5 minutes to 30 minutes (1 minute time bins). This means, like the given MSTR data, the MCNP results will go out to 30 minutes. The earlier time bins were chosen to be smaller as more particles are at these early time bins which will contribute to the time bin. The first few minutes is also when most of the transient occurs so having more time bins means the MCNP results will be high-fidelity when needed. The later time bins were chosen to be larger as less particles are available to contribute to the tally bins and because the power changes less between time intervals and thus high-fidelity data is not required. Figure 4.11 shows the tally and time bin cards used for the MSTR.

```
F14:N 7425
T14  1500000000  3000000000  4500000000  6000000000  7500000000  9000000000
     10500000000 12000000000 13500000000 15000000000 16500000000 18000000000
     19500000000 21000000000 22500000000 24000000000 25500000000 27000000000
     28500000000 30000000000 36000000000 42000000000 48000000000 54000000000
     60000000000 66000000000 72000000000 78000000000 84000000000 90000000000
     96000000000 1.02E+11    1.08E+11    1.14E+11    1.2E+11     1.26E+11
     1.32E+11    1.38E+11    1.44E+11    1.5E+11     1.56E+11    1.62E+11
     1.68E+11    1.74E+11    1.8E+11
```

Figure 4.11 Tally and Time Bin Card Inputs for the MSTR

The tally is a F4 type tally specified for cell 7425. This cell is the cavity of the CAE in the MCNP model. The time bins are as specified in the previous paragraph except the minutes have been converted to shakes. These bins create 45 points which will be output from MCNP.

4.3.2. Physics. Figure 4.12 shows the physics cards used for the MSTR.

```
MODE N P
NPS 1E8
ACT FISSION=N,P NONFISS=P
    DN=BOTH DG=MG DNBIAS=10
PHYS:P 3J -1
MPHYS ON
```

Figure 4.12 Physics Options Used for the MSTR

MODE - As the main particle types of concern are neutrons and photons, they were enabled as particle types to be simulated within the problem.

NPS - 1E8 histories was found to be enough histories to obtain statistically significant results.

ACT - Delayed neutrons and delayed gammas from fission products were modeled and delayed gammas from non-fission interactions were modeled. Delayed neutron emission data was calculated using a mixture of both models and library data. Delayed gamma emission data was modeled using only model data. This option was chosen as individual line-amplitude detail was deemed unnecessary to model the time-dependent delayed gamma tail. Up to 10 delayed neutrons were produced per

delayed neutron interaction to help lower the number of particles required to obtain converged delayed neutron statistics.

PHYS:P - The only input changed from default for the PHYS:P card is the fourth entry which controls photonuclear particle production. This entry was set to -1 so photonuclear particle production is analog meaning one photon interaction per collision is sampled.

MPHYS – Since the ACT card delayed gamma emission calculation requires physics models, the models must be turned on utilizing the MPHYS card.

MXm – This card is not shown as it takes too many lines. Isotopes without available photonuclear interaction cross section data and models had the interaction disabled.

4.3.3. Variance Reduction. Because the data only went out to about 30 minutes, statistically significant results were able to be obtained without the need for additional variance reduction techniques beyond the default. The CUT card was implemented as it is the simplest of the applicable variance reduction methods and did not impact results. Figure 4.13 shows the CUT cards utilized. These cards ended photon and neutron transport after 30 minutes was reached within the simulation as additional results would exceed the MSTR detector data obtained.

```
CUT:N 1.8E+11
CUT:P 1.8E+11
```

Figure 4.13 CUT Card

Past tests with the ACRR where data went out to 3 hours showed the need for more complicated variance reduction methods. It was found the TSPLT card was most effective, decreasing the run-time required by 30% while obtaining similar results. The WWG card was also investigated and was found to increase FOM while keeping accurate results. See Appendix C for an example of a WWOUT file created by a WWG card run for the MSTR.

5. RESULTS

5.1. RAW DATA

Figures 5.1 and 5.2 show the raw delayed particle tail data received from the MSTR and MCNP, respectively.

In Figure 5.1, the CIC is obtaining ample contribution until around 30 minutes when the recorder was shut off. This implies the detector is detecting delayed gammas in addition to delayed neutrons as all delayed neutron precursors would be decayed after about 10 minutes. This is because the longest-lived delayed neutron precursor is bromine 87 which has a half life of 55.6 seconds. This means after 556 seconds or around 9.3 minutes 10 half lives will have occurred, effectively meaning no bromine 87 is left in the system. With no delayed neutron precursors in the system, no delayed neutrons will be produced and thus after 10 minutes if the detector is only detecting neutrons it would not be collecting any data.

It can be clearly seen in Figure 5.2 that the contribution from delayed photons is far greater than that of delayed neutrons, which is expected of the delayed particle tail. It can also be seen that the delayed neutrons die out after about 12 minutes which makes sense because the delayed neutron precursors have a relatively low half-life as mentioned before. Just like the MSTR detector data, the MCNP results are receiving a high contribution of gamma flux even at 30 minutes which is expected at the MSTR due to the decaying of fission products and activated materials.

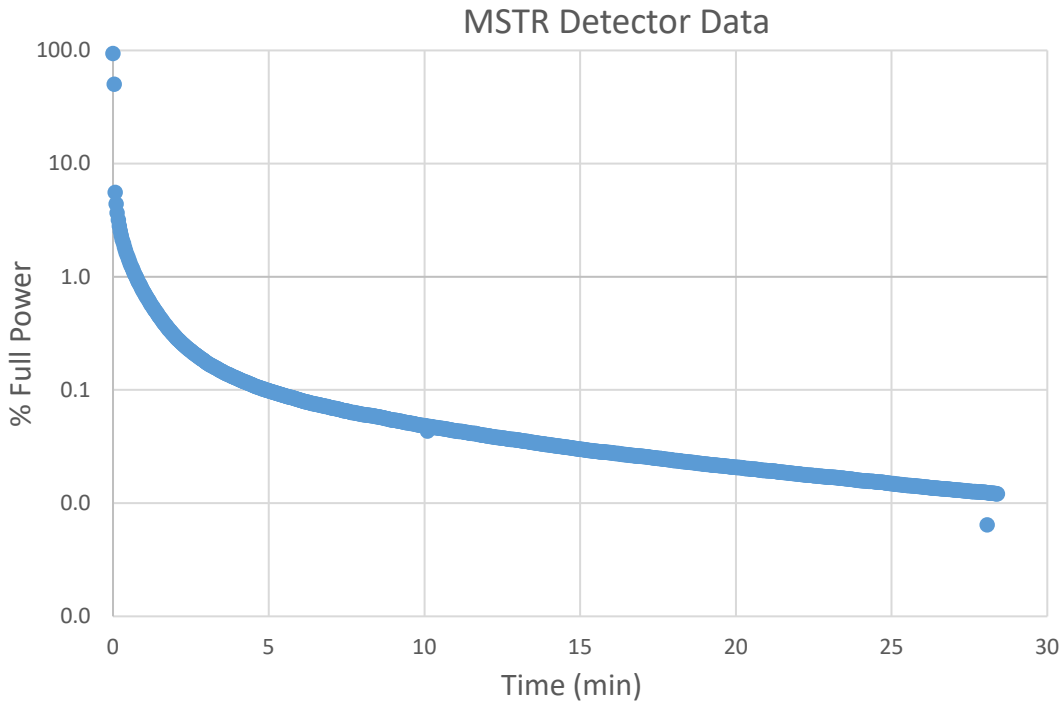

Figure 5.1 Raw MSTR Detector Data

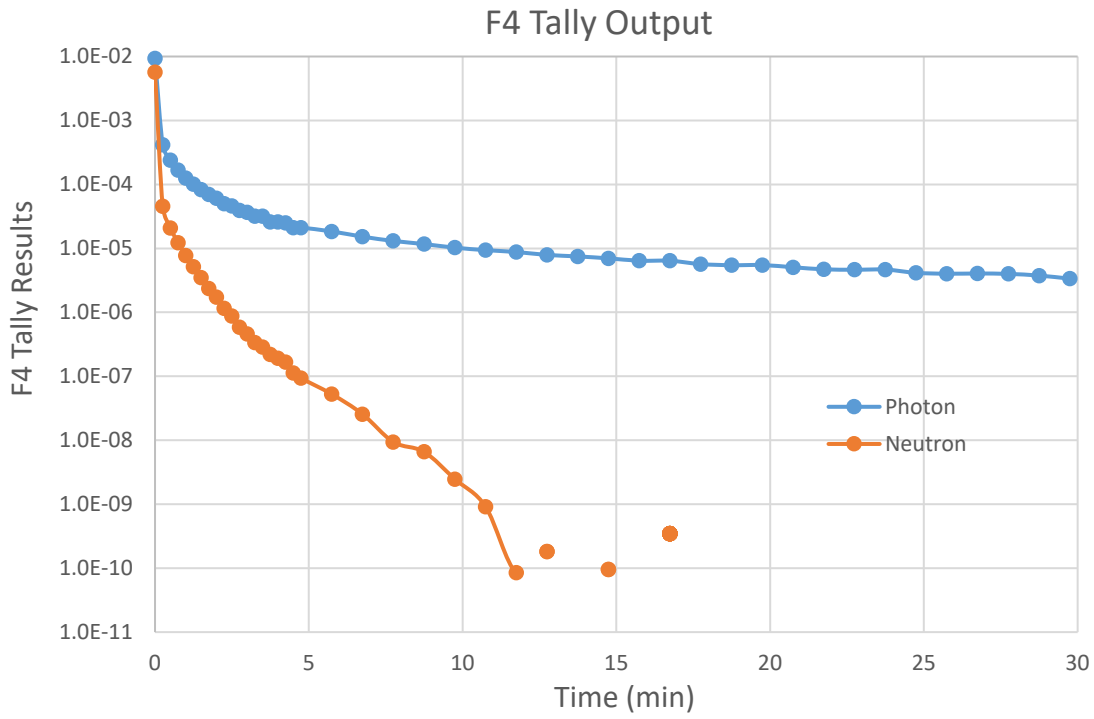

Figure 5.2 F4 Raw Tally Output

Figures 5.3 and 5.4 show the relative tally errors of the photon and neutrons from the F4 tally results, respectively.

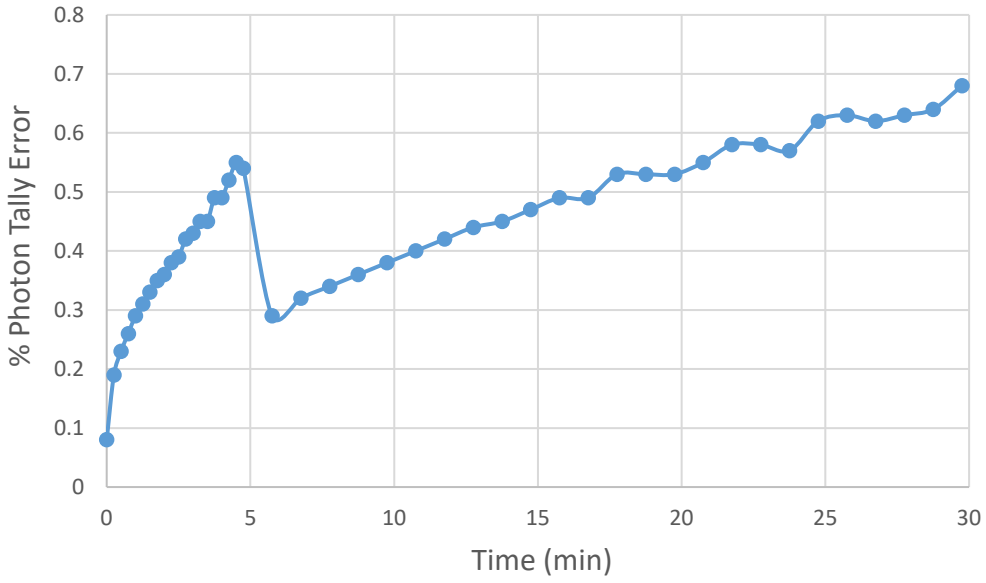

Figure 5.3 F4 Photon Relative Errors

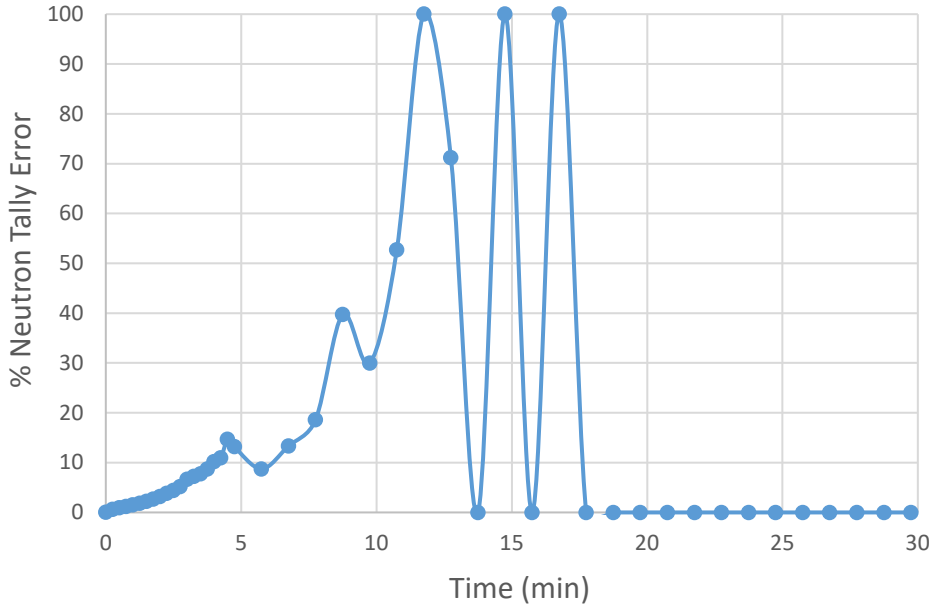

Figure 5.4 F4 Neutron Relative Errors

For all photon result time bins, the errors stay under 0.7%. This error is more than low enough to call the results from the tally reliable. Because the photons provide a far greater contribution to the tally than the neutrons, this means that the total of the tally also has low error. As for neutrons, the relative errors exceed desired values after 5 minutes. This is due to the lack of delayed neutron precursors which means there are fewer particles available to contribute to the tally. For both particle types, the relative tally error drops once the time bins are increased due to a greater likelihood of particles contributing to the time bin. The relationship between increasing time bins and increasing particle counts was found to be directly proportional. Increasing the time bin by a multiple of 4 leads to a reduction in relative tally error by a multiple of 2. This inverse square relationship is the same as is seen with increasing particle count, yet no more particles need be run. This means increasing the length of time bins is a simple yet effective method to improve tally statistics without increasing simulation run-time at the cost of result fidelity.

5.2. NORMALIZED RESULTS

Figure 5.5 shows the normalized results of the MSTR and MCNP data compared to one another. Both sets of data were normalized to 1 and plotted on a lin-log plot. From Figure 5.5, it can be clearly seen that the trend from the MCNP results matches the actual data from the MSTR. Both exhibit a decaying exponential as expected post-shutdown. The MCNP data tends to overpredict the MSTR data. This overprediction becomes more prevalent at later times.

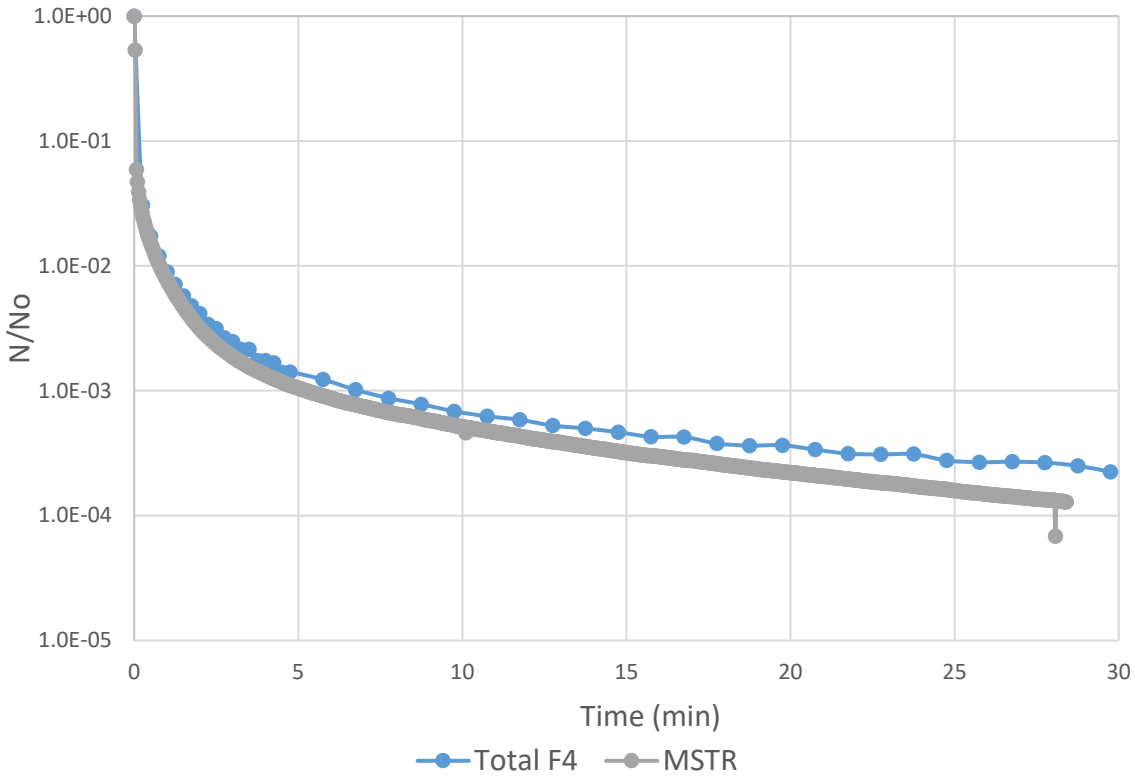

Figure 5.5 Normalized Results Comparison

Figure 5.6 shows the error between the normalized MCNP predicted power and the normalized MSTR data. Before about 15 minutes, the MCNP results agree decently well (errors are below 40%) with the MSTR data. After this, the error continues to increase linearly until it reaches almost 100%. At this point, the MCNP results are double the MSTR data. This overestimation from MCNP provides conservative results which is desired when planning a reactor experiment. The average percent error was found to be 39% and the maximum error was found to be 98%. Possible sources of error are discussed in the next section.

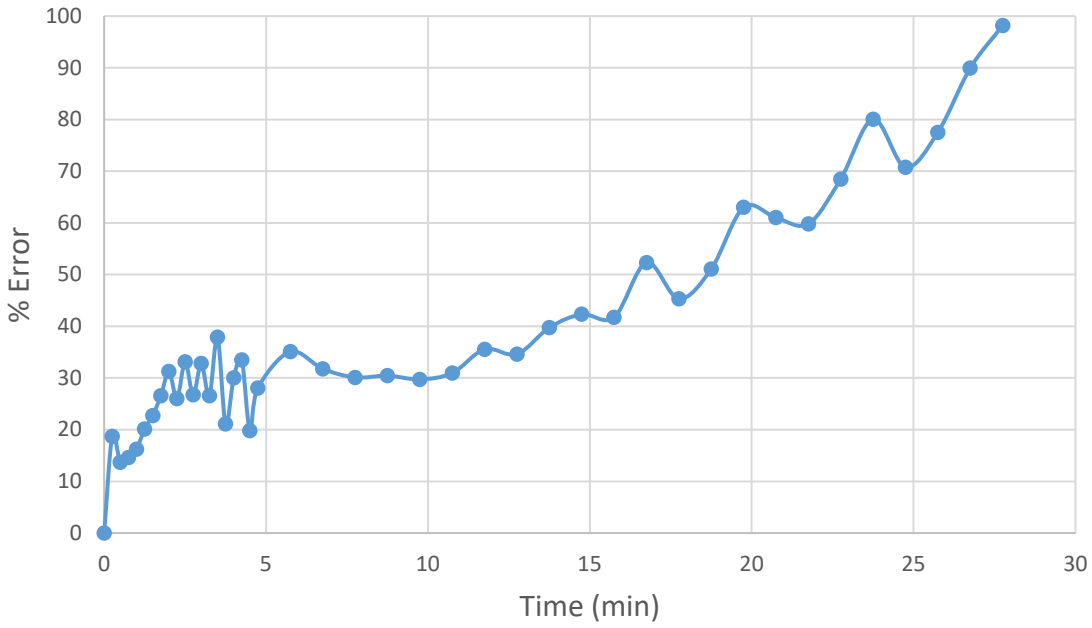

Figure 5.6 Percent Error of MCNP Normalized Results

5.3. SOURCES OF ERROR

There are many sources of error in this specific methodology application. The main sources for these errors are the MCNP geometry and the methodology itself.

5.3.1. MCNP Geometry and Materials. The MCNP MSTR model itself has many issues. First, the model is simplified. Many geometry assumptions are made, and parts are missing such as the bridge and tower assemblies, the stored fuel in the fuel storage pit, the detector guide assemblies, fuel element storage rack, thermal column door assembly, surrounding concrete/air, etc. This can be clearly seen when comparing Figures 4.4 and 4.5. Second, the delayed particle tail tallies were used in the core access element instead of the detector cell. Even when the detector was modeled, it was found to be too difficult to obtain tally contributions even with variance reduction methods due to the distance from the detector to the core. The distance from the center of the core to the

center of the detector is approximately 6ft which means the particles must travel through many feet of water before reaching the detector. Thus, it was determined that utilizing the CAE cavity would best represent the data, however this created an unknown amount of error and may explain why the tally was overpredicting the detector data. The fuel materials also have uncertainties in burnup which would impact the source distribution, creating error in the tallies. As mentioned before, this error is expected to be insignificant due to the low burnup of the MSTR. However, the error caused by the burnup uncertainty should be quantified. Another source of error is in the MCNP model, the reactor goes from all rods up to all rods down instantly. For MSTR, the regulating rod is mechanically coupled to the rod drives and thus does not drop upon shutdown. This rod would take about 1 minute to fully insert from the time of shutdown. Unfortunately, there is not a way to capture this time-dependent geometry within MCNP. The regulating rod accounts for 7% of the total reactivity insertion during shutdown so this could be a large source of error. Another error is that when the source was captured and created, the rod heights did not quite match the actual rod heights when the reactor was shutdown. The difference between the simulated and actual rod heights were under 1%, but it would impact the source distribution and thus tallies. It should also be noted that during high particle runs, it was found that particles would be lost in the geometry. A correction for this error was unable to be found in the time given. It is not expected that this geometry error had a noticeable impact on results, but this should be quantified.

5.3.2. Methodology. As for the methodology itself, it was assumed no delayed neutrons would be created from non-fission events. This assumption was deemed acceptable as the MSTR does not have any materials which would create delayed

neutrons from non-fission products. There is no beryllium or lithium in or near the core which would contribute (n, xn) reactions. Also, the delayed neutrons do not contribute much to the total tally contribution so it is expected this change would have a minimal impact. The methodology is also limited by the accuracy of the delayed particle modeling capability of MCNP. As explored in the Section 2 of this paper, the capability does appear to be accurate but any deviation from perfect accuracy would introduce error. Another source of error would be the choice to disable photonuclear interaction cross sections for isotopes without available photonuclear interaction data or models. The option of utilizing alternative isotope photonuclear interaction data should be explored to find the impact on computation time and results. In addition to these, the source capture process introduces error. The voxels had around 5% error on average and the energy distribution F4 tally results had around 2% error on average. The FMESH process also introduces some error by integrating the result over the voxel although it is expected that utilizing 450,000 voxels depreciated this error. Another source of error would be that the MCNP model was not at secular equilibrium before shutdown. This would greatly change the isotopic distribution in the reactor and thus greatly impact the delayed particles which would be emitted from the reactor. Finally, the CIC detector data technically is not meant to include gammas. This detector does have a small compensating voltage applied to eliminate gamma noise at low powers. The error caused by this could be quantified.

6. CONCLUSIONS AND FUTURE WORK

6.1. CONCLUSIONS

The methodology is computationally expensive due to delayed particle and photonuclear particle production modeling. Many more particles must be run to converge tally bins at late times due to lack of particle contribution. Also, the use of the PHYS:P and ACT cards limit the simulation to a single thread on a Central Processing Unit (CPU). This limitation can be somewhat ignored utilizing MPI tasks, but this process is difficult and only available to users with access to large HPC machines. Variance reduction techniques such as WWG, TSPLT, and CUT are recommended to lower the number of particles which must be run to achieve acceptable statistics at later time bins.

Although the method is computationally expensive, it does model the reactor delayed particle tail trend following a shutdown. Even with the plethora of sources of error, the results are within 45% during the first 15 minutes and then within 100% beyond that. These results are promising, especially because there was no method for modeling the delayed particle tail before this. This work will assist in allowing researchers to better estimate the energy deposition due to the reactor pulse or irradiation itself instead of the delayed particle tail. It should also be noted that the normalized MCNP results overestimating the MSTR detector data is better than the MCNP results underestimating the MSTR data as it means the results are conservative.

6.2. FUTURE WORK

The future work includes lowering the number of error sources for a more reliable validation and future work after validation.

For lowering the number of error sources, creating a less simplified model of the MSTR and/or tallying on the CIC detector instead of the CAE would be a better comparison of the normalized data. An alternative option to this would be to utilize a portable detector in the CAE to obtain data more comparable to the MCNP results. The errors caused by ignoring delayed neutrons from non-fission interactions should also be quantified. This impact is expected to be minimal as no lithium or beryllium is in or near the MSTR core. The error caused by ignoring electrons/alphas/etc. in the simulation should also be quantified, but this is expected to be minimal and would likely greatly increase run-time. To resolve the regulating rod issue, MSTR data would need to be re-done with the reactor leaving the regulating rod out during shutdown. The MSTR geometry errors should be corrected to ensure particles will no longer be lost. Finally, the MSTR data could be re-recorded with a wide-range uncompensated ion chamber (UIC) to ensure the data is accounting for all the gammas, but this detector is unavailable at MSTR. The FMESH TYPE = SOURCE mesh should be optimized to find if there is an optimal voxel size for all reactors which would properly capture the source distribution while also minimizing the number of voxels. Minimizing the number of voxels would reduce the required run-time to achieve converged voxels, reduce the complexity of the source conversion process, and reduce the complexity of the source itself which would lead to more efficient simulations.

As for future work after validation, the future goal is to prove this methodology is dependable enough so that experimenters may apply energy deposition (F6) tallies to a modeled experiment package to quantify the energy deposition to the package from the delayed particle tail. For pulse reactor experiments especially, this would assist in experimenters being able to quantify the energy deposited into a package from the pulse itself as opposed to the delayed particle tail. The outputs of the F6 tally would become inputs to a thermomechanical modeling program to find the expected material temperatures of an experiment package. These temperatures could then be compared to thermocouple data from a pulse experiment to complete the methodology validation.

APPENDIX A.

MESHTAL FILE FORMAT

C This MESHTAL file was created after following the steps from Section 4.1 utilizing the FMESH
C from Figure 4.8. The full file could not be included due to its length.

mcnp version 6.mpi ld=09/19/18 probid = 06/03/22 11:00:50

mstr 130T core zero power critical case

Number of histories used for normalizing tallies = 100000000.00

Mesh Tally Number 4

neutron mesh tally.

C The values below are the midpoints of the voxels from least to greatest.

Tally bin boundaries:

X direction: -12.00 -11.74 -11.48 -11.22 -10.96 -10.70 -10.44 -10.18 -9.92 -9.66…

Y direction: -25.00 -24.72 -24.44 -24.16 -23.88 -23.60 -23.32 -23.04 -22.76 -22.48…

Z direction: -32.00 -28.80 -25.60 -22.40 -19.20 -16.00 -12.80 -9.60 -6.40 -3.20…

Energy bin boundaries: 0.00E+00 1.00E+36

C Below are the midpoint X, Y, Z values for a certain voxel along with the source point tally results and
C the relative error of the results.

X	Y	Z	Result	Rel Error
-11.870	-24.860	-30.400	0.00000E+00	0.00000E+00
-11.870	-24.860	-27.200	0.00000E+00	0.00000E+00
-11.870	-24.860	-24.000	0.00000E+00	0.00000E+00
-11.870	-24.860	-20.800	0.00000E+00	0.00000E+00
-11.870	-24.860	-17.600	0.00000E+00	0.00000E+00
-11.870	-24.860	-14.400	0.00000E+00	0.00000E+00
-11.870	-24.860	-11.200	0.00000E+00	0.00000E+00
-11.870	-24.860	-8.000	0.00000E+00	0.00000E+00

…

APPENDIX B.

SDEF FILE FORMAT

```
C This SDEF was created after converting the MESHTAL file and F4/E4 results from Section 4.1.
C The full file could not be included due to its length.

SDEF PAR=D1 POS=FPAR=D2 ERG=D3

C

C SI1/SP1 split up source distribution into Z slices to speed sampling

SI1 L N N N N N N N N N N N N N N N N N N N

SP1  1.90E-02 4.42E-02 4.51E-02 4.23E-02 3.15E-02

    7.15E-02 7.55E-02 6.49E-02 3.14E-02 6.17E-02

    6.25E-02 4.37E-02 4.70E-02 8.04E-02 7.44E-02

    4.90E-02 3.19E-02 4.87E-02 4.49E-02 3.04E-02

C

DS2 S 4 5 6 7 8 9 10 11 12 13 14 15 16 17 18 19 20

     21 22 23

C

C SI3/SP3 are energy distribution

C SI3 is energy bins, SP3 is normalized F4/E4 results

SI3 L  1.39E-10    1.00E-09    5.00E-09    1.00E-08    3.00E-08

      7.00E-08    1.00E-07    1.52E-07    2.00E-07    4.14E-07

      6.00E-07    8.00E-07    1.13E-06    3.06E-06    5.04E-06

      8.32E-06    1.37E-05    2.26E-05    3.73E-05    6.14E-05

      1.01E-04    1.67E-04    2.75E-04    3.54E-04    4.54E-04

      5.83E-04    7.49E-04    9.61E-04    1.09E-03    1.23E-03

      1.40E-03    1.58E-03    1.80E-03    2.03E-03    2.31E-03

      2.61E-03    2.96E-03    3.35E-03    3.80E-03    4.31E-03

      4.88E-03    5.53E-03    6.27E-03    7.10E-03    8.05E-03

      9.12E-03    1.03E-02    1.17E-02    1.33E-02    1.50E-02

      1.70E-02    1.93E-02    2.19E-02    2.48E-02    2.61E-02

      2.81E-02    3.18E-02    4.09E-02    5.25E-02    6.74E-02

      8.65E-02    1.11E-01    1.43E-01    1.83E-01    2.35E-01
```

```
     3.02E-01    3.88E-01    4.39E-01    4.98E-01    5.64E-01
     6.39E-01    7.24E-01    8.21E-01    9.30E-01    1.05E+00
     1.19E+00    1.35E+00    1.74E+00    2.23E+00    2.87E+00
     3.68E+00    4.72E+00    6.07E+00    7.79E+00    1.00E+01
     1.19E+01    1.35E+01    1.49E+01    1.69E+01    2.00E+01
C
SP3  4.75E-06    2.21E-04    4.25E-03    1.18E-02    7.74E-02
     1.34E-01    5.11E-02    3.63E-02    1.28E-02    2.04E-02
     9.28E-03    7.04E-03    7.96E-03    2.18E-02    1.06E-02
     1.05E-02    1.06E-02    1.08E-02    1.09E-02    1.13E-02
     1.12E-02    1.17E-02    1.16E-02    5.85E-03    5.69E-03
     5.95E-03    5.86E-03    6.12E-03    3.11E-03    2.98E-03
     3.12E-03    2.97E-03    3.14E-03    2.95E-03    3.23E-03
     3.01E-03    3.21E-03    2.95E-03    3.18E-03    3.12E-03
     3.14E-03    3.18E-03    3.13E-03    3.31E-03    3.20E-03
     3.24E-03    3.32E-03    3.62E-03    3.49E-03    3.31E-03
     3.43E-03    3.58E-03    3.86E-03    3.91E-03    1.53E-03
     2.21E-03    4.86E-03    6.68E-03    8.52E-03    9.28E-03
     1.08E-02    9.62E-03    1.26E-02    1.17E-02    1.42E-02
     1.70E-02    1.82E-02    9.20E-03    1.03E-02    1.13E-02
     1.21E-02    1.30E-02    1.37E-02    1.34E-02    1.25E-02
     1.40E-02    1.55E-02    3.20E-02    3.08E-02    3.02E-02
     1.95E-02    1.42E-02    8.56E-03    3.75E-03    1.15E-03
     1.95E-04    4.52E-05    1.25E-05    1.69E-06    0.00E+00
C
C From SI4/SP4 on, these are the source distribution
C SI4 are the FMESH voxel midpoints, SP4 is normalized results of FMESH
C This distribution is for the Z slice -30.4
```

C Each slice contains 22,500 points

SI4 L 2.95 12.1 -30.4

2.43 12.1 -30.4

-2.51 12.1 -30.4

2.69 12.66 -30.4

2.69 15.74 -30.4

-2.77 12.1 -30.4

-1.47 12.38 -30.4

2.43 12.66 -30.4

2.69 12.1 -30.4

1.39 12.38 -30.4

…

C

SP4 3.72E-04

3.68E-04

3.67E-04

3.58E-04

3.44E-04

3.36E-04

3.24E-04

3.24E-04

3.24E-04

3.20E-04

…

APPENDIX C.

WWOUT FILE FORMAT

C This WWOUT file was creating using the WWG and MESH card seen below.

```
WWG 14 0 0 J J J J 0
MESH  GEOM=XYZ ORIGIN=-50 -30 -35
      REF=2.95  12.1  -30.4
      IMESH=30   JMESH=20  KMESH=175
      IINTS=2    JINTS=2   KINTS=2
```

C 8 voxels were created, maximizing contribution to the F14 tally.

C Comments have been added above values to help the reader understand where they are from.
C These comment lines would need to be removed before using this WWOUT file. Extra spaces
C were also added between values to better comment the file.

C HEADER

1 1 2 10 06/03/22 11:00:50

1 1

C IINTS JINTS KINTS OriginX OriginY OriginZ

2.0000 2.0000 2.0000 - 50.000 - 30.000 - 35.000

1.0000 1.0000 1.0000 1.0000

C OriginX IINTS IMESH

-50.000 .0000 30.000 1.0000

C OriginY JINTS JMESH

-30.000 2.0000 20.000 1.0000

C OriginZ KINTS KMESH

-35.000 2.0000 175.00 1.0000

C The below values are the importance values given to the voxels

100.00

9.6573 3.1474 3.8761 0.50000 92.657 0.0000

71.316 67.101

100.00

0.0000 0.15321E+06 0.0000 37006. 0.0000 0.0000

0.0000 0.0000

BIBLIOGRAPHY

[1] Lum, E. S. & Boland, E. J. (2022, April 11). Delayed Particle Tail Modeling Interview. personal.

[2] *Reactor shutdown: Condition & scram*. Nuclear Power. (2022, February 8). Retrieved June 3, 2022, from https://www.nuclear-power.com/nuclear-power/reactor-physics/reactor-operation/reactor-shutdown/

[3] Werner, C. J. (editor) (2017). MCNP Users Manual - Code Version 6.2. LA-UR-17-29981.

[4] Tutt, J. R., Mckinney, G. W., & Wilcox, T. A. (2016). 1. *Proc. of the American Nuclear Society ANTPC, Santa Fe, NM September 27th*.

[5] Wilcox, T. A., & Mckinney, G. W. (2015). MCNP Delayed-Particle Library–Release 5. *Transactions*, *113*(1), 1021-1024.

[6] Tutt, J. R., McKinney, G. W., Wilcox, T. A., & McMath, G. E. (2016). MCNP 6.2. 0 Delayed-Particle Production Improvements. *Transactions of the American Nuclear Society*, *114*(1), 330-333.

[7] McKinney, G. W. (2012, April). 5. In Proceedings of IEEE Nuclear Science Symposium and Medical Imaging Conference, Anaheim, CA, October.

[8] Durkee, J. W., James M. R., McKinney G. W., Waters L. S. & Goorley T. (2012). The MCNP6 Delayed-Particle Feature. *Nuclear Technology*, 180:3, 336-354, DOI: 10.13182/NT12-22.

[9] England, T. R., & Rider, B. F. (1995). *Evaluation and compilation of fission product yields 1993* (No. LA-SUB--94-170). Los Alamos National Lab.

[10] Jurado, B., & Schmidt, K.-H. (n.d.). *A General Description of Fission Observables*. GEF. Retrieved June 3, 2022, from http://www.khschmidts-nuclear-web.eu/GEF.html

[11] Wilson, W. B., England, T. R., George, D. C., Muir, D. W., & Young, P. G. (1995). *Recent development of the CINDER90 transmutation code and data library for actinide transmutation studies* (No. LA-UR-95-2181; CONF-9509162-5). Los Alamos National Lab., NM (United States).

[12] Durkee Jr, J. W., James, M. R., McKinney, G. W., Trellue, H. R., Waters, L. S., & Wilson, W. B. (2009). Delayed-gamma signature calculation for neutron-induced fission and activation using MCNPX, Part I: Theory. *Progress in Nuclear Energy*, *51*(8), 813-827.

[13] Moreno, M. A., & Parma, E. J. (2019). *Method for Calculating Delayed Gamma-Ray Response in the ACRR Central Cavity and FREC-II Cavity Using MCNP* (No. SAND2019-8746). Sandia National Lab.(SNL-NM), Albuquerque, NM (United States).

[14] De Stefano, R., Pérot, B., Carasco, C., & Simon, E. (2020). Simulation of delayed gamma rays from neutron-induced fissions using MCNP 6.1. In *EPJ Web of Conferences* (Vol. 225, p. 06007). EDP Sciences.

[15] Jazbec, A., Pungerčič, A., Kos, B., Ambrožič, K., & Snoj, L. (2021). Delayed gamma radiation simulation in case of loss of water event using Monte Carlo method. *Nuclear Engineering and Design*, *378*, 111170.

[16] Werner, C. J. (2002). Simulation of delayed neutrons using MCNP. *Progress in Nuclear Energy*, *41*(1-4), 385-389.

[17] Meulekamp, R. K., & van der Marck, S. C. (2006). Calculating the effective delayed neutron fraction with Monte Carlo. *Nuclear science and engineering*, *152*(2), 142-148.

[18] Sellers, M. T., Goorley, J. T., Corcoran, E. C., & Kelly, D. G. (2012). A Preliminary Comparison of MCNP 6 Delayed Neutron Emission from(235) U and Experimental Measurements. *Transactions of the American Nuclear Society*, *106*, 813-816.

[19] Los Alamos National Laboratory. (n.d.). *Lib80x—Library based on ENDF/B-VIII.0*. Retrieved June 6, 2022, from https://nucleardata.lanl.gov/ace/lib80x

[20] Richardson, B., Castano, C. H., King, J., Alajo, A., & Usman, S. (2012). Modeling and validation of approach to criticality and axial flux profile experiments at the Missouri S&T Reactor (MSTR). *Nuclear engineering and design*, *245*, 55-61.

VITA

Elijah James Boland was born in Kansas City, Missouri on April 17, 2000. He attended schools in the Lee's Summit R-VII school district and graduated from Lee's Summit West High School with an International Baccalaureate Career-related Program certificate in May 2018. The following August he entered the Missouri University of Science & Technology and in May 2021 received the degree of Bachelor of Science in Nuclear Engineering. He entered the graduate program for Missouri University of Science & Technology in August 2021 and received a Master of Science Degree in Nuclear Engineering in July 2022.